



Kinetic Alfvén Waves Excited by Multiple Free Energy Sources in the Magnetotail

K. C. Barik , S. V. Singh , and G. S. Lakhina

Indian Institute of Geomagnetism Navi Mumbai, 410218, India; kcbarik17@gmail.com

Received 2022 August 12; revised 2023 April 24; accepted 2023 April 24; published 2023 July 3

Abstract

The generation of kinetic Alfvén waves (KAWs) is investigated through a three-component theoretical model incorporating ion beam and velocity shear as the sources of free energy in a non-Maxwellian κ -distributed plasmas. The model considers Maxwellian distributed background ions, drifting-Maxwellian beam ions, and κ -electrons as its constituent species. It is found that the combination of either positive velocity shear with counter-streaming beam ions or parallel streaming beam ions with negative velocity shear favors the excitation of KAWs. The effect of the κ -parameter on the excitation of KAWs under the combined energy sources is explored. The effect of plasma parameters such as number density, propagation angle, and temperature of plasma species on the real frequency and the growth rate of KAWs are examined. For the plasma parameters pertinent to the magnetotail region of Earth's magnetosphere, the model is able to produce KAWs in the frequency range of $\approx(5-67)$ mHz, which matches well with the recent 'Time History of Events and Macroscale Interactions during Substorms (THEMIS)' observations in the near-Earth magnetotail region.

Unified Astronomy Thesaurus concepts: [Solar wind \(1534\)](#); [Space plasmas \(1544\)](#); [Alfven waves \(23\)](#)

1. Introduction

Kinetic Alfvén waves (KAWs) have been paid much attention for the last three decades (Hasegawa 1976) after the pioneering work of A. Hasegawa. It is one of the waves responsible for the particle energization (Goertz & Boswell 1979) and explains the formation of aurora (Hasegawa 1976; Hui & Seyler 1992; Thompson & Lysak 1996). In tokamak plasma, KAWs provide the energy for particle heating across the boundary (Hasegawa 1977). It is believed that KAWs play a dominant role in the ionosphere-magnetosphere coupling and perpendicular ion heating of the ionosphere. KAWs are attributed to explain the perpendicular ion heating in coronal holes and fast solar wind due to stochastic heating (Chandran et al. 2010). Further, as they have a very small perpendicular spatial scale, it is found that KAWs can explain the energy dissipation from the large to small scales of the energy cascade spectrum (Schekochihin et al. 2009; Kumar et al. 2015; Makwana et al. 2015). Broadband KAWs are considered to be one of the drivers for precipitation of outer radiation belt electrons (Chaston et al. 2018). The interaction of KAWs with ions leads to transverse Earthward ion heating (Chaston et al. 2012, 2014). Recent studies have found that KAWs play a dominant role in particle energization at the formation of dipolarization fronts (Ganguli et al. 2018; Ukhorskiy et al. 2022). Further, KAWs undergo mode conversion to electron acoustic waves at the transition region, where the cold ionospheric electron density matches the hot magnetospheric density, which provides another possible mechanism for the formation of discrete aurora (Shi et al. 2018).

The fundamental magnetohydrodynamic (MHD) mode named "Alfvén wave" (Alfvén 1942) gets modified at a very small transverse spatial scale with the addition of the kinetic effect, and this is referred to as KAWs. This kinetic effect

appears in the system under two conditions: (i) In cold electron plasma, at a scale length comparable to the electron inertial scale, when the thermal speed of electrons is much smaller than Alfvén speed of the medium, these waves are called shear kinetic Alfvén waves (SKAWs; Goertz & Boswell 1979; Lysak & Carlson 1981). SKAWs are observed at altitudes below $4-5 R_E$ (R_E is the radius of Earth) in Earth's magnetosphere. (ii) On the other hand, in hot electron plasma, at a spatial scale comparable to the ion gyroradius, when the electron thermal speed is much larger than Alfvén speed, these waves are called KAWs (Hasegawa & Chen 1976; Lysak & Carlson 1981). KAWs are observed above $4-5 R_E$ in Earth's magnetosphere. Note that in both cases the spatial scale of KAWs is defined by the perpendicular wavelength of the wave. The cartoon depicted in Figure 1 describes the appearance of the kinetic effect with the conditions mentioned and the dispersion relations at their respective limits (Barik 2021). The characteristic behavior of the newly formed KAW changes drastically. Unlike the MHD Alfvén waves, where both the ions and electrons follow the field lines and move along with them, the ions due to their large gyroradius detach from the field lines, while the electrons still follow the field lines in the case of KAWs. This charge separation creates a parallel electric field along the direction of the background magnetic field that adds an extra feature to KAWs (Gershman et al. 2017). In contrast to the MHD Alfvén waves that show parallel propagation, the KAWs propagate nearly perpendicular to the ambient magnetic field (Barik et al. 2019a). Further, KAWs exhibit right-handed polarization that distinguishes them from other plasma waves like electromagnetic ion cyclotron waves (Gary 1986; Narita et al. 2020; Moya et al. 2021, 2022).

The signature of KAWs is obtained by looking into the fluctuations in wave electric and magnetic field data from satellite observations. Using Cluster measurement, Salem et al. (2012) found that the small-scale turbulent fluctuations in the solar wind match well with the spectrum of KAWs. By implementing reciprocal magnetic variance anisotropy technique, Podesta & TenBarge (2012) compared the theoretical

Appearance of kinetic effects on Alfvén waves

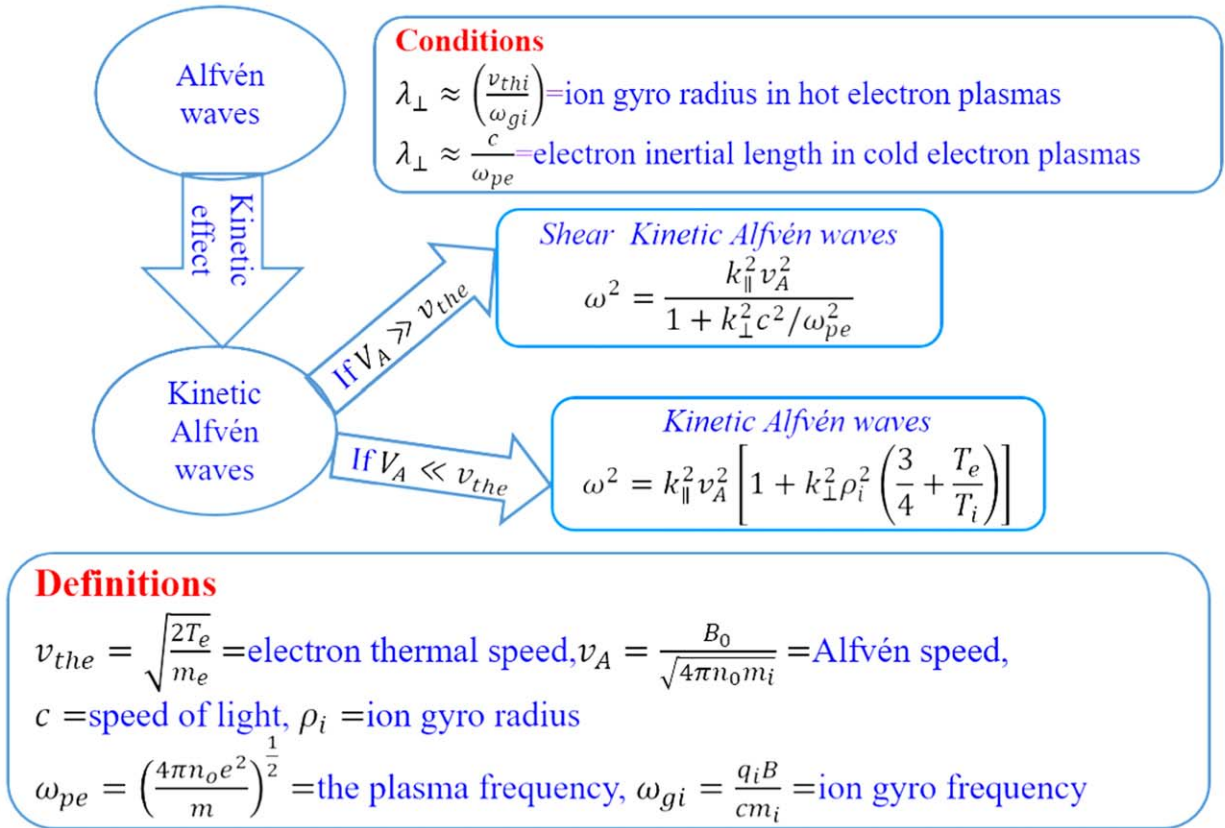


Figure 1. Shows the conditions for the appearance of kinetic effect on Alfvén waves and classification of KAWs with their respective dispersion relations (Barik 2021).

results with Stereo A spacecraft data and predicted that the axisymmetric KAWs in the solar wind are produced by turbulent cascade of Alfvénic fluctuations. Further, in the dissipation range of the turbulence energy cascade, the fluctuations show the behavior of KAWs (Bale et al. 2005). Apart from solar wind and solar atmosphere, KAWs are also observed in different magnetospheric regions, such as, magnetopause (Johnson et al. 2001; Chaston et al. 2005, 2007), magnetosheath, auroral region (Boehm et al. 1990; Louarn et al. 1994; Wahlund et al. 1994), magnetotail, plasma sheet boundary layer (PSBL; Keiling et al. 2000; Keiling et al. 2002; Wygant et al. 2002; Keiling et al. 2005; Duan et al. 2012), and central plasma sheet (Keiling et al. 2001) using sounding rocket and data from various satellites, e.g., Viking, Freja, Fast Auroral Snapshot, Time History of Events and Macroscale Interactions during Substorms (THEMIS), and Cluster. Evidence of KAWs is also found during the main phase of geomagnetic storms (Moya et al. 2015). Further, Van Allen Probe data shows that KAWs are generated due to magnetospheric compression by interplanetary shock (Malaspina et al. 2015). Plasma species directly interact with KAWs and exchange energy with them as observed from Magnetospheric Multiscale (MMS) Mission (Gershman et al. 2017). More recently, Zhang et al. (2022) carried out the first-ever statistical analysis of KAWs using 3 yr of THEMIS spacecraft data from 2008–2010. They have estimated the occurrence of KAWs in the magnetotail regions such as the tail lobe and PSBL with respect to variations in various plasma

parameters and varying geomagnetic conditions like quiet and active periods. Their analysis shows that KAWs have a temporal scale of $\sim(15\text{--}25)$ s, which indicates a frequency range of $\approx(40\text{--}67)$ mHz. Further, their probability of occurrence is larger in the regions having $\beta < 0.1$, i.e., the PSBL and tail lobes. Also, the evidence of KAWs is found both in the quiet time ($AE < 200$ nT) and substorm interval ($AE > 200$ nT); however, the substorm interval pulse has higher Poynting flux as compared to the quiet interval. The theoretical model presented in this article discusses various aspects of this observation of KAWs.

Various sources of free energy exist in the solar atmosphere, planetary environment, and different regions of Earth's magnetosphere. For example, ion beams are evidenced in the solar corona, solar flares, solar wind, and planetary environments (Simnett 1995; Zastrow 2016; Procházka et al. 2018; Delamere et al. 2021). From Ulysses spacecraft observations, it has been confirmed that ion beams are also available in both fast and slow solar wind (Goldstein et al. 2010). Oxygen ion beams are also found on the surface of Mars as evidenced from Mars Atmosphere and Volatile Evolution spacecraft data (Zastrow 2016). Further, transverse velocity shear, which is produced by latitudinal variation of velocity, is reported to be in the solar wind using Ulysses data (Schwadron 2002; McComas et al. 2003). More recently, a substantial amount of velocity shear is reported in the solar wind using Parker Solar Probe data (Phan et al. 2020). In addition to the solar and planetary environments, these sources of free energy are also

available in various regions of Earth's magnetosphere. For instance, an ion beam is observed at different magnetospheric regions, such as the bow shock (Meziane et al. 2007), PSBL (Parks et al. 1998; Takada et al. 2005; Zelený 2007), auroral zone (Schriver et al. 1990), magnetotail (DeCoster & Frank 1979), magnetopause, and polar cusp (Grison et al. 2005). From the Geotail spacecraft, both parallel streaming (Earthward) and counter-streaming beam ions are detected at the PSBL region (Takada et al. 2005). Further, counter-streaming H^+ and O^+ ions are also evidenced in Earth's magnetosphere from ISEE 1 satellite observations (Horita et al. 1987). In addition to the above-mentioned transition regions, there are thick boundaries through which the drift velocity of plasma species changes abruptly and gives rise to velocity shear, which is another source of free energy for the excitation of various instabilities and plasma waves. For example, in the PSBL region, an intense ion beam with velocity $V_B = 10^3$ km s $^{-1}$ is found, which varies over the thickness 10^2 – 10^4 km of the PSBL (D'Angelo et al. 1974; McFadden et al. 1998) giving rise to velocity shear $\left[S = \frac{1}{\omega_B} \left(\frac{dV_B}{dx} \right)\right]$ of ~ 0.1 – 1.0 . In the theoretical model discussed in this article, all of the available free energy sources in the tail lobe-plasma sheet boundary (i.e., parallel and counter-streaming beam ions and velocity shear) are included to investigate the excitation of KAWs.

In addition to the above-mentioned sources of free energy, a non-Maxwellian velocity distribution dominates the space plasma environment starting from the solar wind and solar atmosphere to the interplanetary environment. For instance, non-Maxwellian electrons are present in the solar wind found from Ulysses and ISEE observations (Maksimovic et al. 1997; Pierrard & Lemaire 2001; Zouganelis 2008; Štverák et al. 2009; Maksimovic et al. 2021). Further, the electrons in the coronal sources of the solar flare are best fitted by kappa distribution as evidenced from RHESSI (Oka et al. 2013). Also, kappa electrons have been reported in the magnetosphere of Mercury (Christon 1987) and Saturn (Schippers et al. 2008). In addition to that non-Maxwellian distributed plasma species are found in different regions of Earth's magnetosphere, such as the magnetopause (Graham et al. 2021), magnetosheath (Perri et al. 2020), plasma sheet (Kletzing et al. 2003), and magnetotail (Eyelade et al. 2021).

The generation of KAWs in space plasma environments remains relatively unexplored. Earlier studies found that KAWs can be excited by drift-wave instability (Hasegawa 1977). They can also be formed by the resonant mode conversion of hydromagnetic surface waves (Hasegawa & Chen 1976) and are more probable to occur than the drift-wave instability. In the last two decades, a few studies have been carried out that examine the generation of KAWs using the ion beam and velocity shear as potential sources of free energy. For instance, Lakhina (1990, 2008) studied the excitation of KAWs by velocity shear for the plasma parameters of the polar cusp region and found that they fall in the range of ultra-low-frequency waves. He used plasma species having a Maxwellian velocity distribution. More recently, Barik et al. (2019a) investigated the generation of KAWs by velocity shear, where they used the electrons with a non-Maxwellian κ -distribution and compared the results with the expansion phase of geomagnetic storms. Further, they also examined the ion beam driven resonant instability of KAWs in the presence of κ -electrons and showed the effect of the κ -parameter on the excitation of KAWs (Barik et al. 2021). The nonresonant

instability of KAWs by the combined energy sources of ion beam and velocity shear were studied by Barik et al. (2020). However, there have been no such studies, until now, that account for the combined effect of the ion beam and velocity shear in the resonant instability of KAWs. Although Barik et al. (2019b, 2019c) proposed a theoretical model that was devoted to studying the combined effect of the ion beam and velocity shear in the generation of KAWs in Earth's magnetosphere, it was for complete Maxwellian plasmas. Nevertheless, many satellite observations have confirmed that the velocity distribution of plasma species follows a power law having a long energy tail, which is best described by a non-Maxwellian, like a κ -distribution (Vasyliunas 1968; Pierrard & Lazar 2010; Livadiotis 2015a; Lazar et al. 2016). Hence, taking into consideration the non-Maxwellian distribution of plasma species, here we propose a three-component theoretical model composed of background Maxwellian ions, drifting-Maxwellian beam ions, and non-Maxwellian κ -electrons to examine the generation of KAWs by the cumulative energy source of the ion beam and velocity shear in space plasma environments. The paper is organized as follows: Section 2 describes the basic set of equations used for the development of three-component theoretical model for KAWs. In Section 3, the dispersion relation of KAWs is derived. The analytical expressions for the real frequency and growth rate of KAWs are extracted in Section 4. Section 5 describes the numerical results. Finally, the discussion and conclusions of this work are presented in Section 6.

2. Theoretical Model

We consider a three-component theoretical model encompassing background Maxwellian ions (N_i, T_i), non-Maxwellian kappa electrons (N_e, T_e), and drifting-Maxwellian beam ions (N_B, T_B) as its constituent species. Here, N_j and T_j denote the equilibrium number density and temperature of plasma species j , respectively, where j represents background ions, i , electrons, e , and beam ions, B . The equilibrium charge neutrality is given by the condition $N_e = N_i + N_B$. We consider a geometry where the ambient magnetic field is along the z -direction, i.e., $\mathbf{B} = B_0 \hat{z}$, and the wave electric field, \mathbf{E} , and the propagation vector, \mathbf{k} , lie in yz -plane.

The zeroth-order distribution functions for the plasma species are given as follows:

for electrons:

$$f_{0e}(v) = \frac{N_e}{\sqrt{\pi^3} \Theta_e^3} \frac{\Gamma(\kappa + 1)}{\kappa^{3/2} \Gamma(\kappa - 1/2)} \left(1 + \frac{v^2}{\kappa \Theta_e^2} \right)^{-(\kappa+1)} \quad (1)$$

for background ions:

$$f_{0i}(v) = \frac{N_i}{\sqrt{\pi^3} \alpha_i^3} \exp\left(-\frac{v^2}{\alpha_i^2}\right) \quad (2)$$

for beam ions:

$$f_{0B}(v_{\perp}, v_{\parallel}) = \frac{N_B}{\sqrt{\pi^3} \alpha_B^3} \exp\left[-\frac{(v_{\perp}^2 + (v_{\parallel} - V_B(X))^2)}{\alpha_B^2}\right]. \quad (3)$$

Here, Γ is the usual gamma function. The parameter κ indicates the non-Maxwellian nature of electrons, which takes a small value for highly non-Maxwellian electrons (between 2 and 6 in space plasma physics) and a very large value, i.e., ∞

for Maxwellian electrons. Further, $\alpha_j = \left(\frac{2T_j}{m_j}\right)^{1/2}$ is the thermal speed of plasma species having mass m_j . Also, v_\perp and v_\parallel are the perpendicular and parallel components of velocity, respectively, defined with respect to the ambient magnetic field. The generalized thermal speed, Θ_e , of an electron is given by

$$\Theta_e = \left[\left(\frac{\kappa - 3/2}{\kappa} \right) \right]^{1/2} \left(\frac{2T_e}{m_e} \right)^{1/2}. \quad (4)$$

Note that Equation (4) is invalid for $\kappa < 3/2$; hence, Equation (1) is satisfied for all of the κ -parameters with $\kappa > 3/2$. Further, in Equation (3), $V_B(X)$ represents the nonuniform streaming of beam ions, where $X = x + v_y/\omega_{cB}$ is the constant of motion, with $\omega_{cB} = \frac{eB_0}{cm_B}$ representing the cyclotron frequency of beam ions and c is the speed of light. This indicates that ion beams are drifting along the background magnetic field, i.e., the z -direction having a gradient in one of the directions perpendicular to the ambient magnetic field, i.e., the x -direction considered here. This nonuniform streaming along the x -direction gives rise to velocity shear. It is worth mentioning that positive and negative velocity shear are just sign conventions. For instance, in our model, the gradient along the x -direction is considered as positive velocity shear, while that along the negative x -direction is treated as negative velocity shear.

It is worth mentioning that there are two different ways of representing the non-Maxwellian kappa distribution analytically. These are categorized as type-A and type-B as per the explanation given by Lazar et al. (2015, 2016) and Lazar (2021). Both of the representations have their own advantages. In the type-A distribution, the definition of temperature remains the same as in the Maxwellian distribution (Livadiotis 2015a), while the thermal speed of plasma species in this distribution is related to the thermal speed of Maxwellian distribution through kappa parameters. This type of distribution shows an enhanced tail along with an enhanced core (Livadiotis 2015a). On the other hand, in the type-B distribution, the definition of thermal speed remains fixed as in the Maxwellian distribution, whereas the temperature, T_κ , of the plasma species in both distributions is related through kappa parameters. Here, an enhanced tail rather than an additionally enhanced core is found (Olbert 1968). In our theoretical model, the type-A kappa distribution is used, whereas one can use the type-B as well for analysis. Lazar et al. (2016) also mentioned that whether or not an external source of energy has to be taken into account is significant with respect to the two alternative Maxwellian limits of a given κ -distributed data set. The latter case would correspond to a Kappa-A system and the former to a Kappa-B system. In our opinion, for a given κ -distributed data set, it is difficult to decide a priori which of the two kappa distributions to choose. We have considered the Kappa-A distribution for suprathermal electrons, which has a strong theoretical backing by Livadiotis (2015a). However, we would like to point out that though we have selected the Kappa-A distribution here, we could have also used Kappa-B equally well, and the results would not be different. This is true, as long as one does not forget to substitute the quantity T_κ (which is very often misinterpreted as temperature), with the actual, physical temperature in the analysis. Therefore, the results presented here are applicable when the suprathermal electrons are described by a Kappa-A distribution.

It is important to mention here that apart from the form of kappa distribution used in this model, there is another way of representing the kappa distribution as mentioned in Olbert (1968), Livadiotis & McComas (2009), and Livadiotis (2015b). Note that temperature is a fundamental physical quantity. The definition of the temperature of a system remains unchanged under any circumstances, although its value may vary depending on the mean energy of the system. It can be obtained from the distribution function by calculating the second-order moment irrespective of the shape of the distribution functions considered. Hence, one can use either of the forms of the distribution functions, provided the analytical expression is taken care of properly. A detailed discussion on the applicability of these two forms of kappa distribution functions can be found in the textbook by Livadiotis (2017).

The model is derived for a low plasma beta (ratio of thermal to magnetic pressure), $m_e/m_i \ll \beta < 1$. In a low beta plasma environment, the incompressible nature of the wave magnetic field along the ambient magnetic field allows us to write the electric field as the gradient of two different scalar potentials, i.e., one along the perpendicular direction, ϕ , and the other along the parallel direction, ψ . With this notation, the wave electric field can be expressed as (Hasegawa 1976)

$$\mathbf{E} = E_\perp \hat{y} + E_\parallel \hat{z} = -\nabla_\perp \phi - \nabla_\parallel \psi. \quad (5)$$

The perturbed distribution function can be found by solving the linearized Vlasov equation and is given by (Lakhina 2008; Barik et al. 2019b)

$$f_{ij} = \frac{e_j}{m_j} \sum_{n=-\infty}^{+\infty} \sum_{m=-\infty}^{+\infty} \frac{e^{i(n-m)\theta}}{(k_\parallel v_z - \omega + n\omega_{cj})} J_n(\xi_j) J_m(\xi_j) \times (k_\perp M_j \phi + k_\parallel L_j \psi). \quad (6)$$

Here, $J_n(\xi_j)$ and $J_m(\xi_j)$ are the Bessel functions of the order of n and m , respectively, with the argument $\xi_j = \left(\frac{k_\perp v_\perp}{\omega_{cj}}\right)$. A cylindrical coordinate ($v_\perp, \theta, v_\parallel$) is considered, where θ is the angle that the velocity vector makes with the ambient magnetic field. While arriving at the above equation, a perturbation of the form $f_{ij} = \exp(ik_\perp y + ik_\parallel z - i\omega t)$ is considered, where k_\perp and k_\parallel represent the components of wave propagation vector, \mathbf{k} in the perpendicular and parallel direction, respectively, with respect to the ambient magnetic field, and ω is the frequency of KAWs. Further, a local approximation ($L_B k \gg 1$) is assumed to solve the linearized Vlasov's equation. Here, $k = \sqrt{k_\perp^2 + k_\parallel^2}$ is the wavenumber and $L_B = V_B \left(\frac{dV_B}{dx}\right)^{-1}$ is the velocity gradient scale length of beam ions. The coefficients M_j and L_j appearing in Equation (6) are given by (Lakhina 2008; Barik et al. 2019b)

$$M_j = \left(1 - \frac{k_\parallel v_z}{\omega}\right) \left[\frac{\partial f_{0j}}{\partial v_\perp} \cdot \frac{n\omega_{cj}}{k_\perp v_\perp} + \frac{1}{\omega_{cj}} \frac{\partial f_{0j}}{\partial x} \right] + \frac{\partial f_{0j}}{\partial v_z} \frac{n\omega_{cj}}{\omega} \frac{k_\parallel}{k_\perp} \quad (7)$$

$$L_j = \frac{k_\perp v_z}{\omega} \left[\frac{\partial f_{0j}}{\partial v_\perp} \cdot \frac{n\omega_{cj}}{k_\perp v_\perp} + \frac{1}{\omega_{cj}} \frac{\partial f_{0j}}{\partial x} \right] + \left(1 - \frac{n\omega_{cj}}{\omega}\right) \frac{\partial f_{0j}}{\partial v_z}. \quad (8)$$

The term $\left(\frac{1}{\omega_{cj}} \frac{\partial f_{0j}}{\partial x}\right)$ in Equations (7)–(8) appears due to the presence of velocity shear in the theoretical model, in the absence of which they reduce to Equations (7) and (8) of

Barik et al. (2021). Further, f_{0j} is the zeroth-order distribution function of plasma species, which can take the forms as mentioned in Equations (1)–(3) for electrons, background ions, and beam ions, respectively. With the substitution of the proper equilibrium distribution function of plasma species, the respective perturbed distribution functions can be derived as mentioned in the Appendix.

The perturbed number density and the z -component of the current density can be found from the relation

$$n_j = \int d^3v f_{1j}, \quad J_{zj} = \int d^3v v_z f_{1j}. \quad (9)$$

The expressions of n_j and J_{zj} for various plasma species, i.e., electrons, background ions, and beam ions are given in the Appendix. These perturbed quantities are used in Poisson's equation and the z -component of Ampere's law, given by Poisson's Equation:

$$-\nabla_{\perp}^2 \phi - \nabla_{\parallel}^2 \psi = 4\pi \sum_j e_j n_j \quad (10)$$

The z -component of Ampere's law:

$$\frac{\partial \nabla_{\perp}^2 \phi}{\partial z} - \frac{\partial \nabla_{\parallel}^2 \psi}{\partial z} = \frac{4\pi}{c^2} \frac{\partial}{\partial t} \sum_j J_{zj}. \quad (11)$$

3. Dispersion Relation

Now, substituting the respective values of number density, n_j , and the z -component of current density, J_{zj} , of different plasma species from Equations (A4)–(A9) in Equations (10)–(11) and solving for ϕ and ψ , these equations can, in combination, be written as

$$\begin{pmatrix} D_{11} & D_{12} \\ D_{21} & D_{22} \end{pmatrix} \begin{pmatrix} \phi \\ \psi \end{pmatrix} = 0, \quad (12)$$

where the various dispersion coefficients are given by

$$D_{11} = k_{\perp}^2 \left[1 + \left(\frac{\kappa - 1}{\kappa} \right)^{1/2} \left(\frac{\omega_{pe}^2}{\omega_{ce}^2} \right) + \frac{2\omega_{pi}^2}{k_{\perp}^2 \alpha_i^2} (1 - b_i) + \frac{2\omega_{pB}^2 \bar{\omega}}{k_{\perp}^2 \alpha_B^2 \omega} (1 - b_B) \right] \quad (13)$$

$$D_{12} = k_{\parallel}^2 \left[1 + \frac{\omega_{pe}^2}{k_{\parallel}^2 \Theta_e^2} \left\{ \frac{(2\kappa - 1)}{\kappa} + \frac{i\sqrt{\pi} \kappa!}{\kappa^{3/2} \Gamma(\kappa - 1/2)} \left(\frac{2\omega}{k_{\parallel} \Theta_e} \right) \right\} - \frac{\omega_{pi}^2}{k_{\parallel}^2 \alpha_i^2} b_i Z' \left(\frac{\omega}{k_{\parallel} \alpha_i} \right) - \frac{\omega_{pB}^2}{k_{\parallel}^2 \alpha_B^2} b_B Z' \left(\frac{\bar{\omega}}{k_{\parallel} \alpha_B} \right) \left(1 - S \frac{k_{\perp}}{k_{\parallel}} \right) \right] \quad (14)$$

$$D_{21} = k_{\parallel} k_{\perp}^2 \left[1 + \frac{\omega_{pB}^2}{k_{\perp}^2 c^2} b_B S \frac{k_{\perp}}{k_{\parallel}} \right] \quad (15)$$

$$D_{22} = -k_{\parallel} k_{\perp}^2 \left[1 - \frac{\omega_{pe}^2}{c^2 k_{\perp}^2} \left\{ \frac{(2\kappa - 1)}{\kappa} \frac{\omega^2}{k_{\parallel}^2 \Theta_e^2} + \frac{i\sqrt{\pi} \kappa!}{\kappa^{3/2} \Gamma(\kappa - 1/2)} \frac{2\omega^3}{k_{\parallel}^3 \Theta_e^3} \right\} + \frac{\omega_{pi}^2}{c^2 k_{\perp}^2} \left\{ \frac{\omega^2}{k_{\parallel}^2 \alpha_i^2} b_i Z' \left(\frac{\omega}{k_{\parallel} \alpha_i} \right) + \frac{\omega_{pB}^2}{c^2 k_{\perp}^2} \left\{ \frac{\omega^2}{k_{\parallel}^2 \alpha_B^2} b_B Z' \left(\frac{\bar{\omega}}{k_{\parallel} \alpha_B} \right) \left(1 - S \frac{k_{\perp}}{k_{\parallel}} \right) + S \frac{k_{\perp}}{k_{\parallel}} \right\} \right] \right]. \quad (16)$$

Here, $S = \frac{1}{\omega_{pB}} \left(\frac{dV_B}{dx} \right)$ and $\bar{\omega} = (\omega - k_{\parallel} V_B)$ are the velocity shear and Doppler-shifted frequency of the beam ions, respectively, and $b_j = I_0(\lambda_j) \exp(-\lambda_j)$, where $I_0(\lambda_j)$ is the zeroth-order modified Bessel function with $\lambda_j = \left(\frac{k_{\perp}^2 \alpha_j^2}{2\omega_j^2} \right)$. Further, Z is the plasma dispersion function having the form given by Fried (2015), and Z' is its derivative. Now, equating the determinant of the coefficients of ϕ and ψ from Equation (12) to zero, the dispersion relation of KAW is found to be

$$\begin{aligned} & \frac{b_i N_i}{N_e} \left[1 + a_1 - \frac{\omega^2}{k_{\parallel}^2 v_A^2} \frac{N_i}{N_e} \frac{1 - b_i}{\lambda_i} A q_0 \right] \\ & - \frac{\omega^2}{k_{\parallel}^2 c_s^2} \left[C'_R + i(1 + a_1) C_I - \frac{\omega^2}{k_{\parallel}^2 v_A^2} \frac{N_i}{N_e} \frac{1 - b_i}{\lambda_i} A (C_R + i C_I) \right] \\ & = \frac{2\omega^2}{k_{\parallel}^2 \alpha_i^2} \frac{N_i}{N_e} (1 - b_i), \end{aligned} \quad (17)$$

where the coefficients are expressed as

$$a_1 = \frac{N_B}{N_e} \frac{\beta_B b_B}{2\lambda_B} S \frac{k_{\perp}}{k_{\parallel}} \quad (18)$$

$$q_0 = 1 + \frac{N_B}{N_i} \frac{m_i}{m_B} \frac{S k_{\perp}}{b_i k_{\parallel}} \quad (19)$$

$$A = 1 + \frac{N_B}{N_i} \frac{T_i}{T_B} \frac{\bar{\omega}}{\omega} (1 - b_B) \quad (20)$$

$$C_R = \frac{(2\kappa - 1)}{(2\kappa - 3)} + \frac{N_B}{N_e} \frac{T_e}{T_B} b_B \left(1 - S \frac{k_{\perp}}{k_{\parallel}} \right) \quad (21)$$

$$C'_R = \frac{(2\kappa - 1)}{(2\kappa - 3)} + \frac{N_B}{N_e} \frac{T_e}{T_B} \times \left\{ b_B \left(1 - \frac{\bar{\omega}}{\omega} \right) + \left(\frac{\bar{\omega}}{\omega} - b_B S \frac{k_{\perp}}{k_{\parallel}} \right) \right\} + a_1 C_R \quad (22)$$

$$C_I = \sqrt{\pi} \frac{\omega}{k_{\parallel} \theta_e} \left[\frac{\kappa!}{\kappa^{3/2} \Gamma(\kappa - 1/2)} \frac{2\kappa}{(2\kappa - 3)} + b_B \frac{N_B}{N_e} \left(\frac{T_e}{T_B} \right)^{3/2} \left(\frac{m_B}{m_e} \right)^{1/2} \frac{\bar{\omega}}{\omega} \left(1 - S \frac{k_{\perp}}{k_{\parallel}} \right) \times \left(\frac{2\kappa - 3}{2\kappa} \right)^{1/2} \exp \left(- \frac{\bar{\omega}^2}{k_{\parallel}^2 \alpha_B^2} \right) \right]. \quad (23)$$

Here, $v_A = \frac{B_0}{\sqrt{4\pi N_e m_i}}$ is the Alfvén speed, and $c_s = \left(\frac{T_e}{m_i} \right)^{1/2}$ is the ion acoustic speed. Further, $\beta_i = (8\pi N_e T_i / B_0^2)$ and

$\beta_B = (8\pi N_e T_B / B_0^2)$ are the ion and beam plasma betas, respectively. It is worth mentioning that while arriving at Equation (17), $\omega^2 \ll \omega_{cj}^2$ is assumed for the low-frequency electromagnetic KAWs. Further, it is also considered that background ions are cold ($\omega \gg k_{\parallel} \alpha_B$), electrons are hot ($\omega \ll k_{\parallel} \alpha_e$, $\lambda_e \rightarrow 0$), and beam ions are hot ($\bar{\omega} \leq k_{\parallel} \alpha_B$). In the absence of beam ion number density (N_B) and damping terms, Equation (17) reduces to

$$\left[b_i - \frac{(2\kappa - 1) \omega^2}{(2\kappa - 3) k_{\parallel}^2 c_s^2} \right] \cdot \left[1 - \frac{\omega^2 (1 - b_i)}{k_{\parallel}^2 v_A^2 \lambda_i} \right] = \frac{2\omega^2(1 - b_i)}{k_{\parallel}^2 \alpha_i^2}, \quad (24)$$

$$\gamma = - \frac{D_I(\omega_r, \mathbf{k})}{\frac{\partial D_R(\omega_r, \mathbf{k})}{\partial \omega_r}} = \frac{\omega_r^2 \left[1 + a_1 - \frac{\omega_r^2 (1 - b_i) N_i}{k_{\parallel}^2 v_A^2 \lambda_i} \frac{N_i}{N_e} A \right] C_I}{\omega_r \{ 2(g_1^2 - 4g_0)^{1/2} \} + k_{\parallel} V_B \frac{N_B}{N_e} (1 - b_B) \left\{ \frac{\omega_r^2 T_i C_R}{k_{\parallel}^2 v_A^2 T_B \lambda_i} - \frac{T_e}{T_B} \left[1 + \frac{N_i T_i b_i \beta_i}{N_e T_e 2\lambda_i} q_0 \right] \right\}}. \quad (31)$$

which is nothing but the dispersion relation that describes the coupling between ion acoustic waves (IAWs) and KAWs in the presence of κ -electrons. In the limit $\kappa \rightarrow \infty$, i.e., for Maxwellian electrons, it reduces to Equation (23) of Lakhina (2008). In the small beta plasma limit, these two waves get decoupled, and two distinct wave modes for KAWs and IAWs are obtained as mentioned in Equations (29) and (30) of Barik et al. (2021). Barik et al. (2020) quantified the plasma beta parameter for the coupling of KAWs with IAWs both for Maxwellian and κ -electrons.

4. Real Frequency and Growth Rate of KAWs

Equation (17), as it is a complex quantity, can be written as a combination of the real and imaginary parts and expressed as

$$D_R(\omega, \mathbf{k}) + iD_I(\omega, \mathbf{k}) = 0, \quad (25)$$

where

$$D_R(\omega, \mathbf{k}) = \frac{\omega^4}{k_{\parallel}^4 v_A^4} \left[\frac{N_i (1 - b_i)}{N_e \lambda_i} A C_R \right] - g_1 \frac{\omega^2}{k_{\parallel}^2 v_A^2} + \frac{N_i b_i \beta_i T_e}{N_e 2 T_i} (1 + a_1) \quad (26)$$

$$D_I(\omega, \mathbf{k}) = - \frac{\omega^2}{k_{\parallel}^2 v_A^2} \left[1 + a_1 - \frac{\omega^2 (1 - b_i) N_i}{k_{\parallel}^2 v_A^2 \lambda_i} \frac{N_i}{N_e} A \right] C_I \quad (27)$$

$$g_1 = \left[C'_R + \frac{N_i}{N_e} (1 - b_i) \frac{T_e}{T_i} \left\{ 1 + \frac{N_i b_i \beta_i}{N_e 2\lambda_i} A q_0 \right\} \right]. \quad (28)$$

The real frequency can be obtained from the solution of $D_R(\omega, \mathbf{k}) = 0$ and is given by

$$\omega_r^2 = \frac{k_{\parallel}^2 v_A^2}{2} \frac{\lambda_i N_e}{(1 - b_i) A N_i C_R} [g_1 \pm (g_1^2 - 4g_0)^{1/2}] \quad (29)$$

where

$$g_0 = \left(\frac{N_i}{N_e} \right)^2 \frac{b_i \beta_i T_e (1 - b_i)}{2 T_i \lambda_i} (1 + a_1) A C_R. \quad (30)$$

The growth rate of KAW is found to be

It is important to mention here that the real frequency and growth rate expressions, as mentioned in Equations (29) and (31), contain both of the free energy sources, i.e., ion beam and velocity shear. In the absence of velocity shear, Equations (29) and (31) reduce to Equations (35) and (37) of Barik et al. (2021), i.e., for a purely beam ion effect. Further, for beam ions with low streaming velocity, i.e., $k_{\parallel} V_B \ll \omega$, Equations (29) and (31) reduce to Equations (40) and (41) of Barik et al. (2019a). Usually, resonance in a plasma system occurs when the thermal speed of a plasma species becomes comparable to the phase velocity of the wave, and the wave particles interact through collisionless Landau damping. In the model considered here, resonance occurs under the condition, $(\omega - k_{\parallel} V_B) \leq k_{\parallel} \alpha_B$, i.e., when the Doppler-shifted phase velocity of KAWs approaches the thermal speed of beam ions.

5. Numerical Analysis

The physical plasma parameters of Equations (29) and (31) are normalized as follows: real frequency (ω_r) and growth rate (γ) are normalized with respect to the beam ion cyclotron frequency, ω_{cB} . The number density of background ions (N_i) and beam ions (N_B) are normalized by the electron number density (N_e). Temperatures of electrons (T_e) and background ions (T_i) are normalized by the temperature (T_B) of beam ions. The streaming velocity (V_B) is normalized with the thermal velocity of beam ions, α_B , and the normalized velocity shear is expressed as $S = 1/\omega_{cB} (dV_B/dx)$. The normalized real frequency (ω_r/ω_{cB}) and normalized growth rate (γ/ω_{cB}) are plotted with the normalized perpendicular wavenumber ($\lambda_B^2 = \frac{k_{\perp}^2 \alpha_B^2}{2\omega_{cB}^2}$) for numerical analysis.

The variations of normalized real frequency (ω_r/ω_{cB}) and normalized growth rate (γ/ω_{cB}), with the square of the normalized perpendicular wavenumber, $\lambda_B = \frac{k_{\perp}^2 \alpha_B^2}{2\omega_{cB}^2}$, for

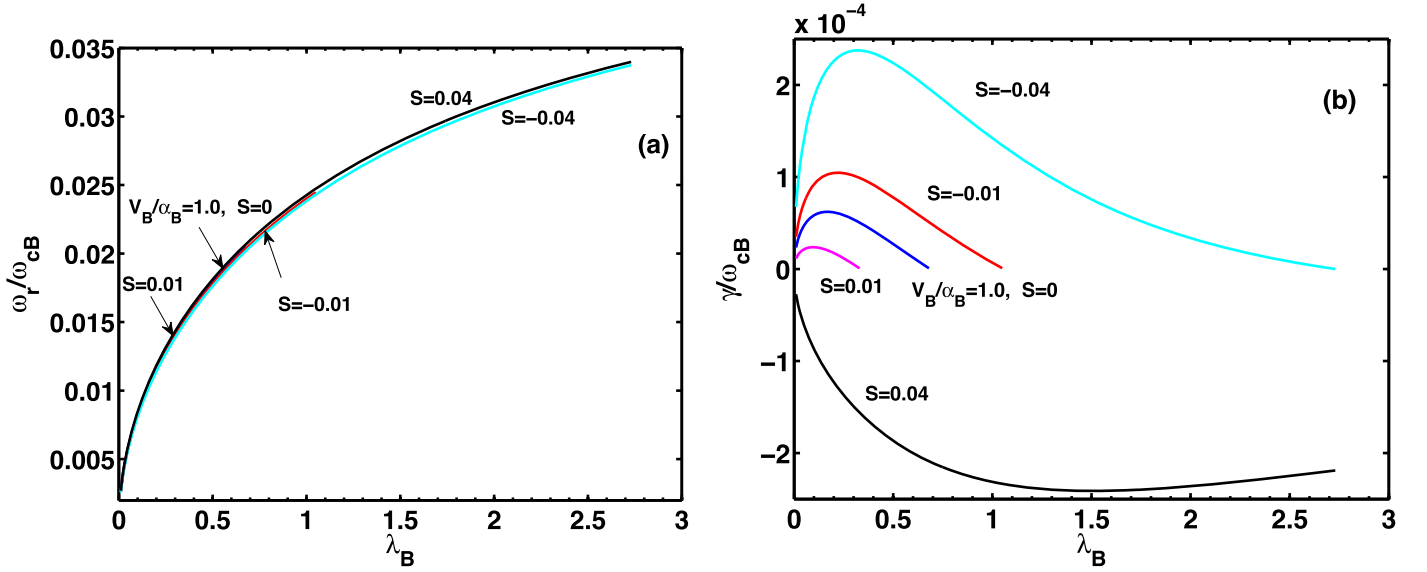


Figure 2. Resonant instability of KAWs by ion beam and velocity shear: variation of (a) normalized real frequency and (b) normalized growth rate vs. square of the perpendicular wavenumber, $\lambda_B = \frac{k_\perp^2 \alpha_B^2}{2\omega_{cB}^2}$, for the plasma parameters, $V_B/\alpha_B = 1.0$, $N_B/N_e = 0.18$, $\beta_i = 0.001$, $k_\parallel/k_\perp = 0.05$, $T_i/T_B = 0.016$, $T_e/T_B = 0.6$, $\kappa = 3$, and various values of velocity shear S as mentioned along the curves.

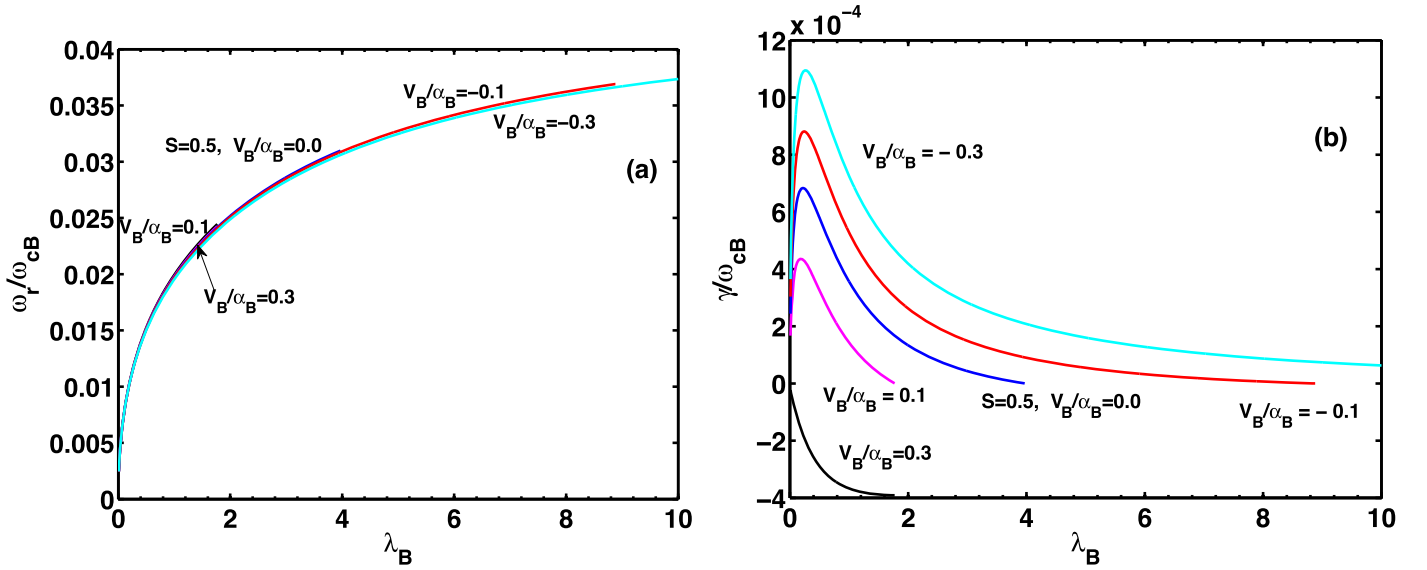


Figure 3. Resonant instability of KAWs by ion beam and velocity shear: variation of (a) normalized real frequency and (b) normalized growth rate vs. square of the perpendicular wavenumber, $\lambda_B = \frac{k_\perp^2 \alpha_B^2}{2\omega_{cB}^2}$, for the plasma parameters, $S = 0.5$, $N_B/N_e = 0.18$, $\kappa = 2$, $k_\parallel/k_\perp = 0.05$, $\beta_i = 0.001$, $T_i/T_B = 0.016$, $T_e/T_B = 0.6$, and various values of ion beam velocity, V_B/α_B , as listed along the curves.

different values of velocity shear at a fixed value of ion beam velocity, $V_B/\alpha_B = 1.0$, and other plasma parameters are shown in Figure 2. It can be seen that parallel streaming beam ions as a single source ($S = 0$ curve) can excite the resonant instability of KAWs with a significant growth rate (cf. blue curve in Figure 2(b)). With this current scenario, when positive velocity shear increases gradually from zero, the growth rate of KAWs starts reducing and after a critical value of positive velocity shear, there is no growth; only the damping of KAWs is seen. From numerics, the critical value of positive velocity shear is found to be 0.019. There is a negligible change in the real frequency curves; however, the peak real frequency increases. In contrast, when velocity shear increases in a similar fashion in the opposite direction, which we termed “negative velocity

shear,” the reverse effect occurs, which leads to the generation of KAWs with a larger growth rate as compared to the single source of beam ions or combined sources of positive velocity shear and parallel streaming of beam ions. Hence, from the above analysis, it can be inferred that in the presence of parallel streaming beam ions, positive velocity shear has a stabilizing effect, whereas negative velocity shear favors the resonant instability of KAWs and produces a larger growth rate.

In the presence of positive velocity shear, the effect of parallel and counter-streaming beam ions (defined with respect to the direction of the ambient magnetic field) on the real frequency and growth rate of KAWs in the resonant instability is illustrated in Figure 3. Positive velocity shear alone as a source is able to excite the resonant instability of KAWs

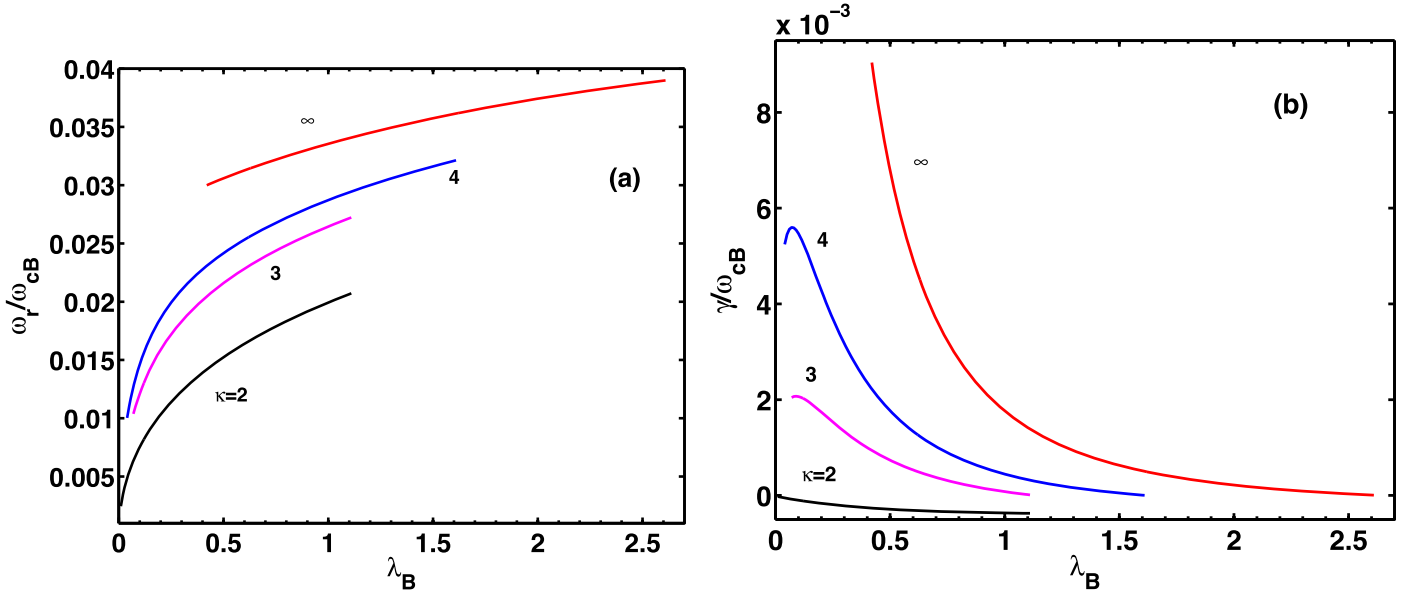


Figure 4. Resonant instability of KAWs by ion beam and velocity shear: variation of (a) normalized real frequency and (b) normalized growth rate vs. square of the perpendicular wavenumber, $\lambda_B = \frac{k_{\perp}^2 \alpha_B^2}{2\omega_{cB}^2}$, for the plasma parameters, $S = 0.5$, $V_B/\alpha_B = 0.3$, $N_B/N_e = 0.18$, $k_{\parallel}/k_{\perp} = 0.05$, $\beta_i = 0.001$, $T_i/T_B = 0.016$, $T_e/T_B = 0.6$, and various values of the κ -parameter as listed along the curves.

(cf. blue curve in Figure 3(b)). Note that a positive value of V_B/α_B indicates the parallel streaming beam ions here, while a negative value represents the counter-streaming beam ions. It is found that in the presence of positive velocity shear, the growth rate along with a wave unstable region decreases with an increase in parallel streaming ion beam velocity. The wave growth is seen up to a value of $V_B/\alpha_B = 0.27$; thereafter, only damping of the wave occurs. However, the real frequency increases slightly. In contrast, however, the growth rate of KAWs enhances with gradual enhancement in counter-streaming ion beam velocity. The wave unstable region also increases gradually. Hence, the analysis indicates that parallel streaming beam ions with positive velocity shear have a stabilizing effect on the KAW resonant instability, while the counter-streaming beam ions with positive velocity shear favor the wave excitation and produce a larger growth rate of KAWs. This confirms the results presented in Figure 2.

The effect of the κ -parameter on the real frequency and growth rate of KAWs when positive velocity shear and parallel streaming beam ions are considered as the source of free energy is depicted in Figure 4. The damping of KAWs is observed for the considered values of plasma parameters and $\kappa = 2$. With the increase in κ -parameter, the growth rate as well as the real frequency of KAWs increase significantly. The wave unstable region (range of λ_B for which growth of KAWs is found) remains nearly the same for $\kappa = 2$ and 3; however, it increases further with an increase in the κ -parameter. The peak real frequency and growth rate are at a maximum for $\kappa = \infty$, i.e., for Maxwellian electrons. Also, the wave unstable region is relatively large as compared to highly non-Maxwellian electrons ($\kappa = 2$). Hence, it can be concluded that the presence of Maxwellian electrons facilitates the growth of KAWs, while the non-Maxwellian κ -electrons hinder the growth and limit the wave unstable region. The effect of the κ -parameter on the other combination of free energy sources is also investigated. For $S = 0.5$ and $V_B/\alpha_B = -0.3$ and with other plasma parameters the same as in the above analysis, growth of KAWs

is obtained for each value of the κ -parameter starting from 2, and the growth rate and wave unstable region increase with an increase in the κ -parameter. The same trend continues for the free energy source with $V_B/\alpha_B = 1.0$ and $S = -0.04$ with other plasma parameters remaining the same. However, for other combinations of free energy sources such as $V_B/\alpha_B = 1.0$ and $S = 0.04$, only damping of KAWs is noticed for each value of κ , though the damping decreases with increase in κ -parameter. Even the damping of KAWs persists for $\kappa = \infty$, i.e., for Maxwellian electrons. However, if the velocity shear value changes to $S = 0.02$, keeping all other plasma parameters the same as before, the damping of KAWs persists up to $\kappa = 3$, after which a growth in KAWs is found, which increases further for enhancement in the κ -parameter.

In the presence of the combined free energy sources of positive velocity shear, $S = 0.5$ and counter-streaming beam ions, $V_B/\alpha_B = -0.3$, the variations of normalized real frequency and growth rate with λ_B in the resonant instability of KAWs for various values of propagation angle are depicted in Figure 5. It is found that with an increase in k_{\parallel}/k_{\perp} , the peak growth rate of KAWs decreases, while the peak real frequency increases significantly. From the numerics, it is found that for the considered plasma parameters, no growth rate of KAWs is obtained for $k_{\parallel}/k_{\perp} > 0.22$, i.e., for the propagation angle, $\theta < 77^{\circ}.6$. The case of positive velocity shear, $S = 0.5$, and parallel streaming beam ions with, $V_B/\alpha_B = +0.3$, keeping all other plasma parameters fixed, as for Figure 5, is also investigated. It is found that the resonant instability of KAWs is not excited for $k_{\parallel}/k_{\perp} > 0.043$, i.e., for propagation angle, $\theta < 87^{\circ}.5$. However, the growth rate of the KAWs increases with an increase in propagation angle beyond $87^{\circ}.5$. It is seen that the features are completely reversed when the effect is studied by the combined source of parallel streaming beam ions, $V_B/\alpha_B = 1.0$ and negative velocity shear, $S = -0.04$ as noticed from the real frequency and growth rate variations shown in Figure 6. It is observed that, unlike the previous results shown in Figure 5, both the peak growth rate and real

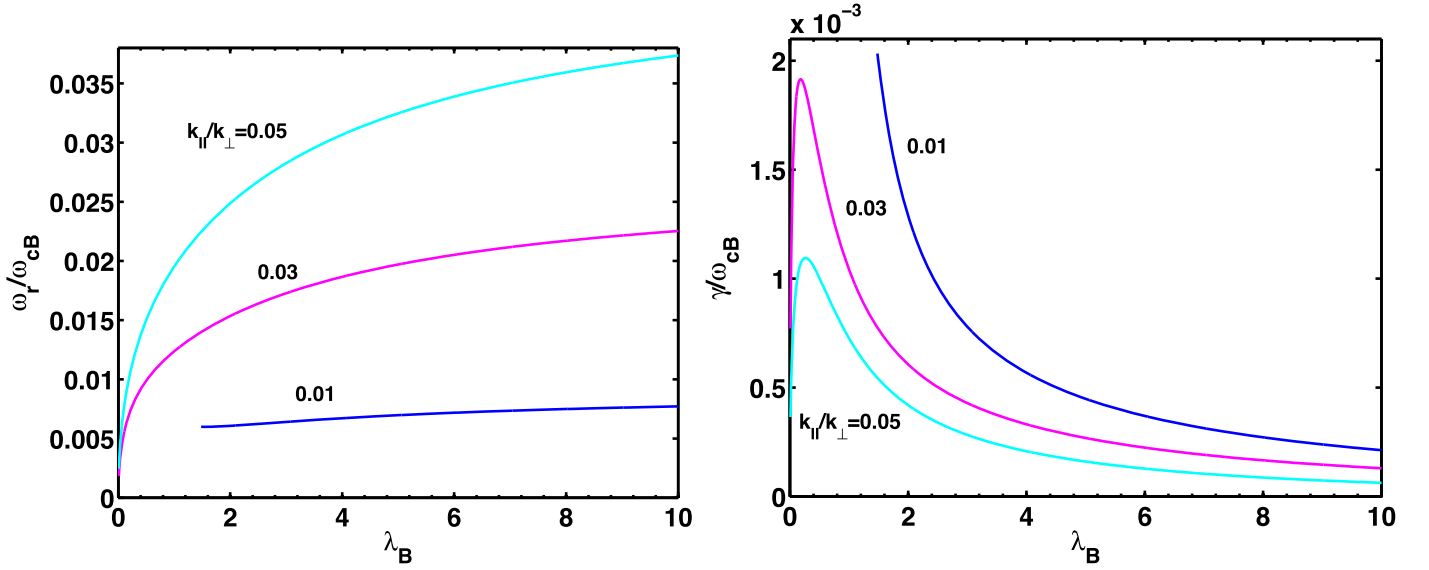


Figure 5. Resonant instability of KAWs by ion beam and velocity shear: variation of (a) normalized real frequency and (b) normalized growth rate vs. square of the perpendicular wavenumber, $\lambda_B = \frac{k_{\perp}^2 \alpha_B^2}{2\omega_{cB}^2}$, for the plasma parameters, $S = 0.5$, $V_B/\alpha_B = -0.3$, $\kappa = 2$, $N_B/N_e = 0.18$, $\beta_i = 0.001$, $T_i/T_B = 0.016$, $T_e/T_B = 0.6$, and various values of $k_{||}/k_{\perp}$ as listed on the curves.

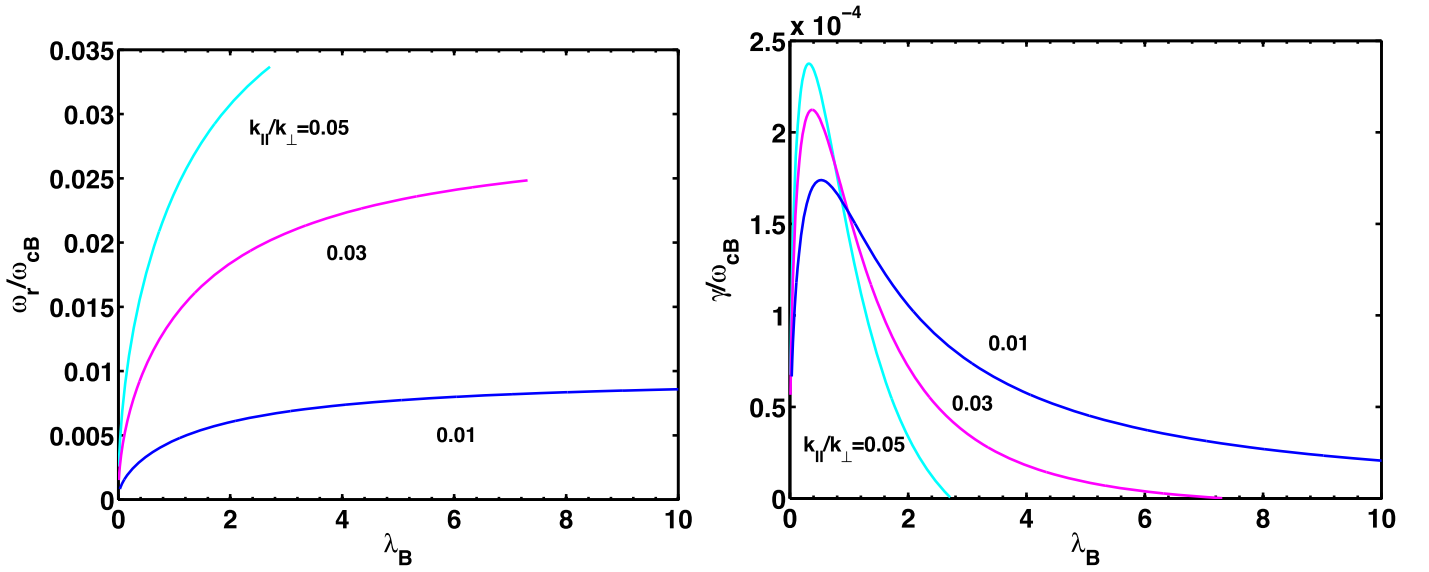


Figure 6. Resonant instability of KAWs by ion beam and velocity shear: variation of (a) normalized real frequency and (b) normalized growth rate vs. square of the perpendicular wavenumber, $\lambda_B = \frac{k_{\perp}^2 \alpha_B^2}{2\omega_{cB}^2}$, for the plasma parameters, $S = -0.04$, $V_B/\alpha_B = 1.0$, $\kappa = 3$, $N_B/N_e = 0.18$, $\beta_i = 0.001$, $T_i/T_B = 0.016$, $T_e/T_B = 0.6$, and various values of $k_{||}/k_{\perp}$ as listed on the curves.

frequency increase gradually with the gradual enhancement in $k_{||}/k_{\perp}$ values. Further, in contrast to the previous case, the wave unstable region decreases gradually with increase in $k_{||}/k_{\perp}$ value. Note that except for κ (which is 3 here), all other fixed plasma parameters remain the same. It is also observed that at smaller λ_B , the changes in real frequency and growth rate are negligible; however, significant changes are noticed at larger λ_B regions. This effect is also examined for parallel streaming beam ions, $V_B/\alpha_B = 1.0$, with positive velocity shear, $S = 0.04$, as the source of free energy. It is found that with such a scenario, wave excitation is possible at a propagation angle very close to perpendicular propagation ($89^\circ.9$), below which only damping of the wave is seen.

Figure 7 shows the variations of normalized real frequency and growth rate with λ_B for different values of electron temperature (normalized by beam ion temperature), T_e/T_B , in the resonant instability of KAWs driven by the combined energy source of positive velocity shear, $S = 0.5$, and counter-streaming beam ions, $V_B/\alpha_B = -0.3$. It is found that both the real frequency and growth rate rise with increase in temperature, T_e/T_B . The range of the wave unstable region also increases with an increase in T_e/T_B . It is noticed that in the smaller λ_B range, the change in real frequency for different T_e/T_B values is nominal, while significant changes are noticed in the larger λ_B range. For the set of plasma parameters (as mentioned in the Figure 7 caption), the threshold value of temperature is found to be $T_e/T_B = 0.113$, below which the

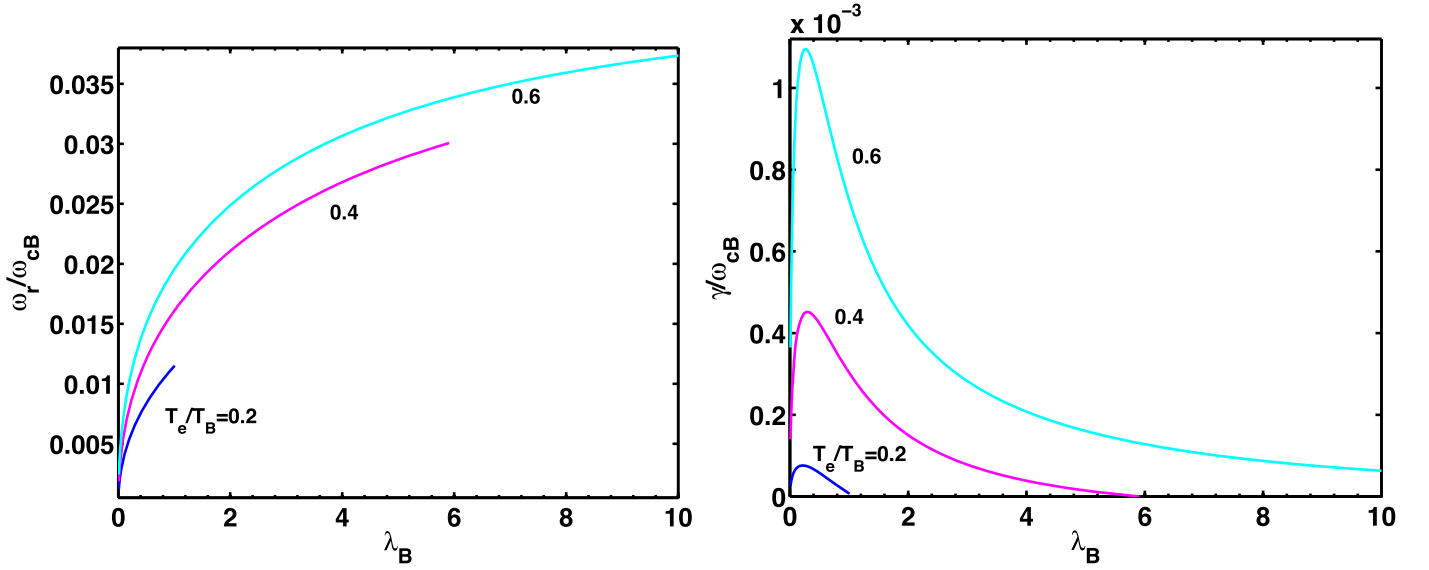


Figure 7. Resonant instability of KAWs by ion beam and velocity shear: variation of (a) normalized real frequency and (b) normalized growth rate vs. square of the perpendicular wavenumber, $\lambda_B = \frac{k_{\perp}^2 \alpha_B^2}{2\omega_{cB}^2}$, for the plasma parameters, $S = 0.5$, $V_B/\alpha_B = -0.3$, $\kappa = 2$, $N_B/N_e = 0.18$, $\beta_i = 0.001$, $k_{\parallel}/k_{\perp} = 0.05$, $T_i/T_B = 0.016$, and various values of T_e/T_B as listed along the curves.

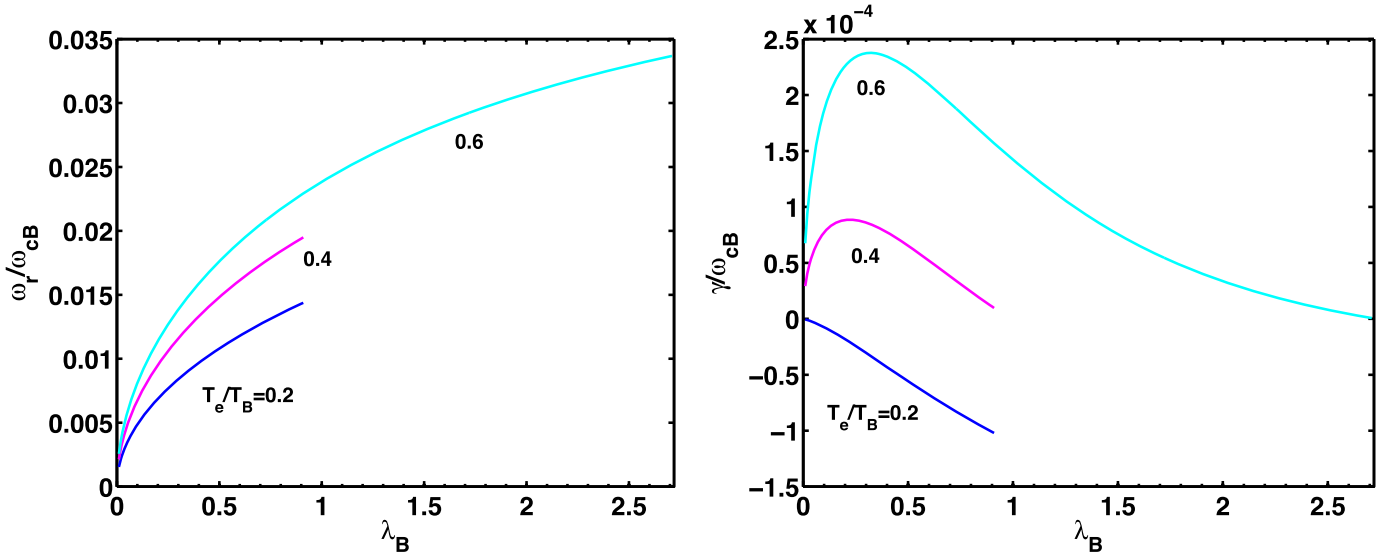


Figure 8. Resonant instability of KAWs by ion beam and velocity shear: variation of (a) normalized real frequency and (b) normalized growth rate vs. square of the perpendicular wavenumber, $\lambda_B = \frac{k_{\perp}^2 \alpha_B^2}{2\omega_{cB}^2}$, for the plasma parameters $S = -0.04$, $V_B/\alpha_B = 1.0$, $\kappa = 3$, $N_B/N_e = 0.18$, $\beta_i = 0.001$, $k_{\parallel}/k_{\perp} = 0.05$, $T_i/T_B = 0.016$, and various values of T_e/T_B as listed along the curves.

excitation of KAWs is not possible. The effect of temperature is also investigated by replacing the counter-streaming beam ions by their corresponding parallel streaming beam ions, keeping all other parameters fixed. It is observed that the trend remains same; however, a relatively high temperature threshold of $T_e/T_B = 0.65$ is required to excite the resonant instability of KAWs.

Figure 8 illustrates the effect of temperature, T_e/T_B , on the normalized real frequency and growth rate of KAWs for the free energy source of parallel streaming beam ions, $V_B/\alpha_B = 1.0$, and negative velocity shear, $S = -0.04$. It can be seen that the features are exactly the same as shown in Figure 7. From the computations, the threshold value of temperature, T_e/T_B , is found to be 0.21 for the set of plasma

parameters considered here. It is found that a relatively high value of temperature threshold, i.e., $T_e/T_B = 3.0$, is required to excite the resonant instability of KAWs when the negative velocity shear is replaced by exactly the same value of positive velocity shear, with all other plasma parameters remaining the same. Hence, negative velocity shear with parallel streaming beam ions creates more favorable conditions for the excitation of KAWs as compared to negative velocity shear with parallel streaming beam ions.

The effect of ion beam number density, N_B/N_e , variations on the real frequency and growth rate of KAWs excited by the combined energy source of positive velocity shear, $S = 0.5$, and counter-streaming beam ions, $V_B/\alpha_B = -0.3$, is delineated in Figure 9. Note that the growth rate and also the wave

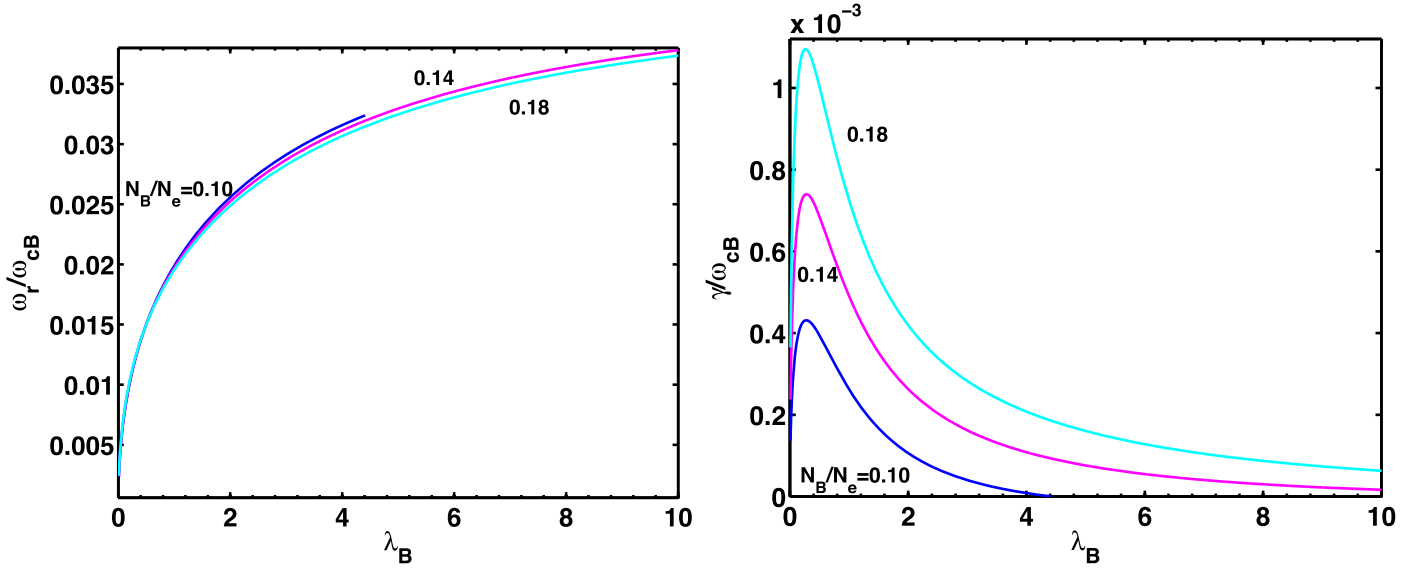


Figure 9. Resonant instability of KAWs by ion beam and velocity shear: variation of (a) normalized real frequency and (b) normalized growth rate vs. square of the perpendicular wavenumber, $\lambda_B = \frac{k_{\perp}^2 \alpha_B^2}{2\omega_{cB}^2}$, for the plasma parameters, $S = 0.5$, $V_B/\alpha_B = -0.3$, $\kappa = 2$, $\beta_i = 0.001$, $k_{\parallel}/k_{\perp} = 0.05$, $T_i/T_B = 0.016$, $T_e/T_B = 0.6$, and various values of N_B/N_e as listed along the curves.

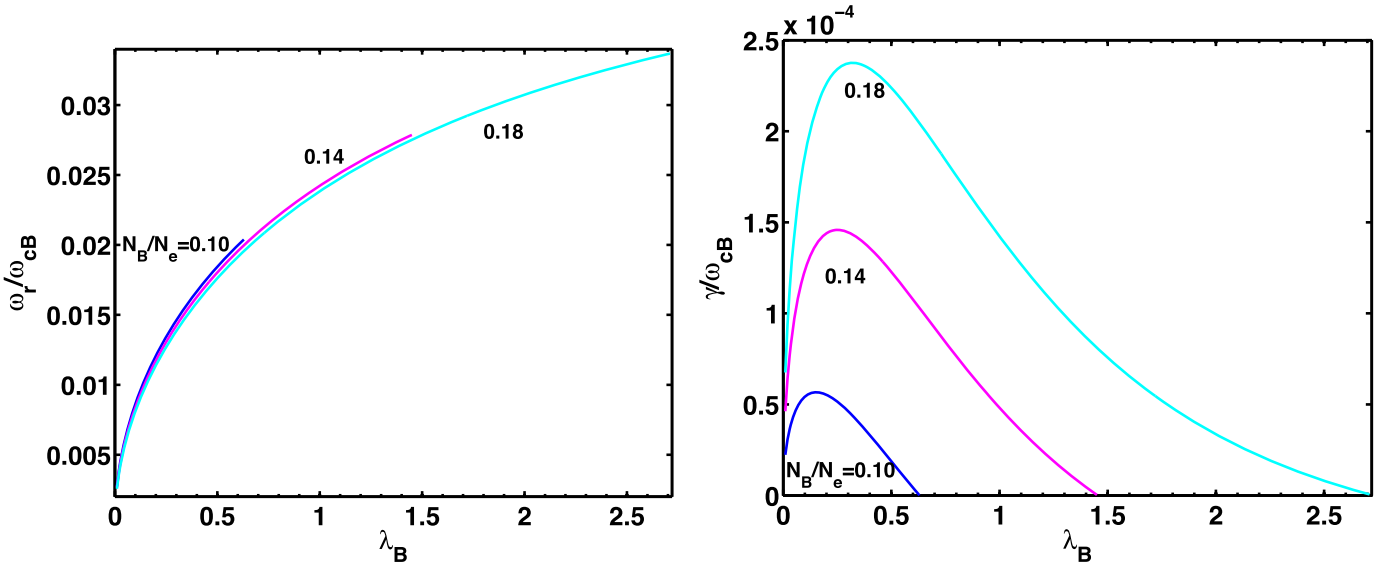


Figure 10. Resonant instability of KAWs by ion beam and velocity shear: variation of (a) normalized real frequency and (b) normalized growth rate vs. square of the perpendicular wavenumber, $\lambda_B = \frac{k_{\perp}^2 \alpha_B^2}{2\omega_{cB}^2}$, for the plasma parameters, $S = -0.04$, $V_B/\alpha_B = 1.0$, $\kappa = 3$, $\beta_i = 0.001$, $k_{\parallel}/k_{\perp} = 0.05$, $T_i/T_B = 0.016$, $T_e/T_B = 0.6$, and various values of N_B/N_e as listed along the curves.

unstable region increase with an increase in ion beam number density, whereas the real frequency (though marginal) decreases with an increase in N_B/N_e . From numerics, the threshold value of ion beam number density is found to be 0.028 for the set of plasma parameters considered here. Replacing the counter-streaming beam ions by the parallel streaming beam ions, $V_B/\alpha_B = 0.3$, for the current set of plasma parameters, it is found that although the features of the real frequency and growth rate curves remain the same, a relatively higher threshold value of 0.23 is required for the excitation of KAWs.

The same trends are seen for the real frequency and growth rate of KAWs when the wave is excited by the combined energy source of parallel streaming beam ions, $V_B/\alpha_B = 1.0$,

and velocity shear, $S = -0.04$, as delineated in Figure 10. This time the wave is excited for a number density threshold value of $N_B/N_e = 0.067$. However, with such a combination of plasma parameters, if negative velocity shear is replaced by a positive velocity shear of $S = 0.04$, it is difficult to excite KAWs: even 30% beam ions are unable to trigger the wave excitation.

The critical value of ion beam velocity, V_B/α_B , and threshold values of propagation angle (k_{\parallel}/k_{\perp}), electron temperature (T_e/T_B), beam ion number density (N_B/N_e) for highly non-Maxwellian electrons ($\kappa = 2$) to Maxwellian electrons ($\kappa = \infty$) for the velocity shear $S = 0.5$, and other fixed plasma parameters, $N_B/N_e = 0.18$, $T_i/T_B = 0.016$, $T_e/T_B = 0.6$, $\beta_i = 0.001$, and $k_{\parallel}/k_{\perp} = 0.05$, is obtained from

Table 1

Critical Value of Ion Beam Velocity, V_B/α_B , in the Presence of Electrons Starting from κ to Maxwellian Electrons for the Plasma Parameters of $N_B/N_e = 0.18$, $S = 0.5$, $T_i/T_B = 0.016$, $T_e/T_B = 0.6$, $\beta_i = 0.001$, and $k_{\parallel}/k_{\perp} = 0.05$

κ -Value	Critical Value of V_B/α_B	Threshold Value of k_{\parallel}/k_{\perp}	Threshold Value of T_e/T_B	Threshold Value of N_B/N_e
2	0.27	0.22	0.113	0.028
3	0.54	0.306	0.052	0.014
4	0.70	0.33	0.043	0.0114
5	0.82	0.342	0.0381	0.0103
∞	0.95	0.374	0.0376	0.0077

Note. The threshold values of propagation angle (k_{\parallel}/k_{\perp}), electron temperature (T_e/T_B), and beam ion number density (N_B/N_e) are computed for $S = 0.5$ and $V_B/\alpha_B = -0.3$, keeping other plasma parameters the same as before.

numerics and depicted in Table 1. It can be seen that while approaching from non-Maxwellian to Maxwellian electrons, the critical value of the ion beam velocity, V_B/α_B , also increases. This indicates that the presence of Maxwellian electrons enhances the critical value of ion beam velocity drastically. Further, setting the source of free energy to be at $S = 0.5$ and $V_B/\alpha_B = -0.3$, the threshold value of other plasma parameters, such as propagation angle (k_{\parallel}/k_{\perp}), electron temperature (T_e/T_B), and number density of beam ions (N_B/N_e) for the excitation of KAWs for electrons with varying κ -parameter, is also found. It is inferred that KAWs are excited at propagation angles close to 90° in the presence of κ -electrons, whereas they can be excited for propagation angles far below 90° when Maxwellian electrons are present in the system. Further, the presence of hot non-Maxwellian electrons is required for the excitation of KAWs, while relatively cold Maxwellian electrons can make the KAWs unstable when free energy sources are the same. Finally, a comparatively larger value of ion beam number density is required in the presence of κ -electrons to excite KAWs as compared to the Maxwellian electrons.

Table 2 represents the critical value of velocity shear (S) and threshold values of electron temperature (T_e/T_B) and beam ion number density (N_B/N_e) for electrons with different κ -parameters when ion beam velocity, $V_B/\alpha_B = 1.0$, is present as the source of free energy with the other set of plasma parameters $N_B/N_e = 0.18$, $T_i/T_B = 0.016$, $T_e/T_B = 0.6$, $\beta_i = 0.001$, and $k_{\parallel}/k_{\perp} = 0.05$. It is found that the critical value of velocity shear varies reciprocally with the κ -parameter, i.e., for electrons with a smaller κ -parameter, the critical value is relatively high and vice versa. Further, fixing the source of free energy at $V_B/\alpha_B = 1.0$ $S = -0.04$ and other plasma parameters the same as before, the threshold value of temperature, T_e/T_B , and number density, N_B/N_e , are computed. It is found that like the previous case, both the temperature of electrons and the number density of the beam ions are inversely related to the κ -parameter.

6. Discussion and Conclusion

The resonant instability of KAWs excited by the combined free energy sources of ion beam and velocity shear is discussed through a three-component theoretical model consisting of Maxwellian background ions, non-Maxwellian κ -electrons, and drifting-Maxwellian beam ions. Note that we have considered

Table 2

Critical Value of Velocity Shear, S , in the Presence of Electrons Starting from κ to Maxwellian Electrons for the Plasma Parameters of $V_B/\alpha_B = 1.0$, $N_B/N_e = 0.18$, $T_i/T_B = 0.016$, $T_e/T_B = 0.6$, $\beta_i = 0.001$, and $k_{\parallel}/k_{\perp} = 0.05$

κ -Value	Critical Value of S	Threshold Value of T_e/T_B	Threshold Value of N_B/N_e
3	0.019	0.21	0.067
4	0.0246	0.167	0.056
5	0.0269	0.150	0.051
∞	0.0326	0.109	0.039

Note. The threshold values of electron temperature (T_e/T_B) and beam ion number density (N_B/N_e) are calculated for $V_B/\alpha_B = 1.0$ and $S = -0.04$, keeping other plasma parameters the same as before.

the type-A kappa distribution, which considers the temperature, a thermodynamic variable, as independent of the kappa index (Livadiotis 2015a). It is found that ion beam and velocity shear, as a single source, are able to excite the resonant instability of KAWs up to significant growth. Further, parallel streaming beam ions with positive velocity shear and counter-streaming beam ions with negative velocity shear both have stabilizing effects on the resonant instability of KAWs. It is found that the combination of positive velocity shear with counter-streaming beam ions or a combination of negative velocity shear with parallel streaming beam ions favors the excitation of resonant instability of KAWs. However, the former combination dominates over the latter and proved to be a more favorable combination of free energy sources to make KAWs unstable. The presence of κ -electrons hinders the KAW growth as compared to Maxwellian electrons in the presence of all possible combinations of free energy sources. When KAWs are primarily excited by positive velocity shear, the addition of counter-streaming beam ions to the system allows the waves to grow for $\theta > 77.6^\circ$, while the addition of parallel streaming beam ions limits the wave growth to $\theta > 87.5^\circ$. In contrast, when the wave is primarily excited by parallel streaming beam ions, the addition of positive velocity shear restricts the wave growth close to perpendicular propagation, as no growth is found for $\theta < 89.9^\circ$. Further, a relatively higher threshold value of electron temperature, T_e/T_B , and larger threshold value of ion beam number density, N_B/N_e , are required to excite the resonant instability of KAWs in the presence of positive velocity shear with parallel streaming beam ions as compared to the case of positive velocity shear with counter-streaming beam ions. It is also found that when KAWs are primarily excited by parallel streaming beam ions and positive velocity shear is added to the system, even the presence of 30% of beam ions is unable to excite the resonant instability of KAWs.

In a recent study, Zhang et al. (2022) carried out the first-ever statistical analysis of KAWs using the THEMIS spacecraft in magnetotail regions. The occurrence of KAWs in varying geomagnetic conditions, like quiet days, and active periods, like geomagnetic substorm days, is analyzed. The evidence of KAWs is found under both conditions; however, the disturbed time KAWs are associated with an enhanced Earthward Poynting flux. Further, the study shows that the probability of observing KAWs is at a maximum in the region with $\beta < 0.1$, i.e., in the magnetotail region. It also reports the signature of KAWs during magnetic reconnection. However, the report is silent about the generation mechanism of KAWs under such conditions and also about the sources of free energy available during that time. In the model discussed here, the

velocity shear exists at different transition regions of Earth's magnetosphere. The value of velocity shear varies under varying geomagnetic conditions. For example, the compression of the dayside magnetosphere due to interplanetary shocks, high stream solar wind, etc. leads to enhancement of the velocity shear at the magnetopause. Further, at the night side, the velocity shear increases as a result of compression of the nightside magnetosphere during the expansion phase of the geomagnetic substorm. Such enhancements of velocity shear would produce a larger growth rate of KAWs and an increased Poynting flux. This is in agreement with the enhanced KAW Poynting flux during substorms as found by Zhang et al. (2022). It is evidenced from many studies that ion beams are ejected as a byproduct during magnetic reconnection at the night side, which travel in the Earthward direction (Zelenyi et al. 2006a, 2006b; Grigorenko et al. 2007; Zelenyi 2007). These beam ions are the source of free energy for various instabilities. In our model, beam ions can excite KAWs up to a significant growth rate. This result may be able to explain the observation of KAWs during magnetic reconnection as observed by Zhang et al. (2022).

From the THEMIS spacecraft, it is found that background ion temperature $T_i \approx (200\text{--}500)$ eV, electron temperature $T_e \approx 500$ eV–3 keV, and plasma beta $\beta < 0.1$ in the magnetotail region (Zhang et al. 2022). Further, a beam ion temperature of $T_B \approx (5\text{--}30)$ keV is noticed. Also, high-speed field-aligned ion beam streaming with $V_B \geq 2000$ km s⁻¹ and low-speed streaming of 600 km s⁻¹ $\leq V_B \leq 1500$ km s⁻¹ with an energy range of ~ 30 keV and 5 keV, respectively, are noticed from Cluster satellites, which makes $V_B/\alpha_B < 2$ (Zelenyi et al. 2006b). We have used an ion beam number density, $N_B/N_e \leq 0.3$, $\beta_i = 0.001$, ion beam velocity of $-0.5 < V_B/\alpha_B < 1.0$, and velocity shear value of $-0.1 < S < 0.5$ for our computations. Further, an ion beam cyclotron frequency of $\omega_{cB}/2\pi = (2.2\text{--}3)$ Hz is considered. Thus, the plasma parameters considered for our computations are well within the range of observations in the magnetotail region where KAWs have been reported.

The maximum normalized growth rate is found to be 0.0019 at $\lambda_B = 0.18$, and the corresponding real frequency is 0.007 for the plasma parameters considered in Figure 5 (magenta curve). The respective un-normalized growth rate and real frequency are 5.7 mHz and 20 mHz, respectively, for $\omega_{cB}/2\pi = 3$ Hz. The resonant instability of KAWs excited by the combined free energy source of positive velocity shear and counter-streaming beam ions is able to generate KAWs with a frequency of $\approx (5\text{--}67)$ mHz and produce a growth rate of KAWs up to $\approx (0.4\text{--}5.7)$ mHz, while the wave is excited in the λ_B range of (0.01–10). The perpendicular wavenumber is calculated to be $k_{\perp} \approx (0.0036\text{--}0.011)$ km⁻¹, and the corresponding wavelength is $\lambda_{\perp} \approx (554\text{--}1745)$ km. The parallel wavenumber is computed using the relation $k_{\parallel}/k_{\perp} = 0.03$ and is given by $k_{\parallel} \approx (0.011\text{--}0.033) \times 10^{-2}$ km⁻¹, and the associated wavelength is $\lambda_{\parallel} \approx (185\text{--}582) \times 10^2$ km.

From the THEMIS observation, Zhang et al. (2022) found the temporal scale of KAWs to be $\sim (15\text{--}25)$ s, which indicates that the observed KAWs lie in the frequency range $\approx (40\text{--}67)$ mHz. The theoretical model discussed here can generate KAWs of frequency $\approx (5\text{--}67)$ mHz when the wave propagation angle is 88.2° , which is within the observed frequency range of KAWs.

Also, the model is able to produce a KAW growth rate of $\approx (0.4\text{--}5.7)$ mHz. Further, the computed perpendicular

wavelength, $\lambda_{\perp} \approx (554\text{--}1754)$ km, lies on the upper side of the observed range of (20–120) km, whereas the parallel wavelength, $\lambda_{\parallel} \approx (185\text{--}582) \times 10^2$ km, falls on the larger side of the observed range (1000–10,000) km relevant to the PSBL region of Earth's magnetosphere (Wygant et al. 2002). Although this model explains the observation of KAWs in the magnetotail of Earth's magnetosphere, it can be applied to other space plasma environments as well, provided that one of the above-mentioned free energy sources is available with a low plasma beta environment there. Further, this theoretical model is not relevant to observation of KAWs at the dipolarization front, as one has to consider different distribution functions (Ganguli et al. 2018). This is beyond the scope of the model discussed here and will be carried out in a future work.

Acknowledgments

G.S.L. thanks Indian National Science Academy, New Delhi for the support under INSA-Honorary Scientist Scheme.

Appendix

This appendix describes the derivation of perturbed distribution functions for electrons, background ions and beam ions. Further, the expressions for the perturbed number density and z-component of current density of the plasma species are obtained using the perturbed distribution functions.

Equation (6) is a generalized expression for the perturbed distribution function that can accommodate equilibrium distribution functions of any form. Simplifying Equation (6) further with the substitution of the equilibrium distribution functions of the form given by Equations (1)–(3), the perturbed distribution functions for electrons, background ions, and beam ions are obtained and given by

for electrons:

$$f_{1e} = -\frac{e}{m_e} \sum_{n=-\infty}^{+\infty} \sum_{m=-\infty}^{+\infty} \frac{J_n(\xi_e) J_m(\xi_e) e^{i(n-m)\theta}}{(k_{\parallel} v_z - \omega + n\omega_{ce})} \times \left[-(\kappa + 1) \left(1 + \frac{v_{\perp}^2}{\kappa \Theta_{\perp e}^2} + \frac{v_{\parallel}^2}{\kappa \Theta_{\parallel e}^2} \right)^{-1} f_{0e} \right] \times \left\{ \left[\left(1 - \frac{k_{\parallel} v_{\parallel}}{\omega} \right) \left(\frac{2v_{\perp}}{\kappa \Theta_e^2} \frac{n\omega_{ce}}{k_{\perp} v_{\perp}} \right) + \frac{n\omega_{ce}}{\omega} \frac{k_{\parallel}}{k_{\perp}} \frac{2v_{\parallel}}{\kappa \Theta_e^2} \right] k_{\perp} \phi + \left[\frac{k_{\parallel} v_{\parallel}}{\omega} \left(\frac{2v_{\perp}}{\kappa \Theta_e^2} \frac{n\omega_{ce}}{k_{\perp} v_{\perp}} \right) + \frac{2v_{\parallel}}{\kappa \Theta_e^2} \left(1 - \frac{n\omega_{ce}}{\omega} \right) \right] k_{\parallel} \psi \right\} \quad (\text{A1})$$

for background ions:

$$f_{1i} = -\frac{e}{m_i} \sum_{n=-\infty}^{+\infty} \sum_{m=-\infty}^{+\infty} \frac{e^{i(n-m)\theta}}{(k_{\parallel} v_z - \omega + n\omega_{ci})} J_n(\xi_i) J_m(\xi_i) \times \left\{ \left[\left(1 - \frac{k_{\parallel} v_{\parallel}}{\omega} \right) \left(\frac{2v_{\perp}}{\alpha_i^2} \frac{n\omega_{ci}}{k_{\perp} v_{\perp}} \right) + \frac{n\omega_{ci}}{\omega} \frac{k_{\parallel}}{k_{\perp}} \frac{2v_{\parallel}}{\alpha_i^2} \right] k_{\perp} \phi + \left[\frac{k_{\parallel} v_{\parallel}}{\omega} \left(\frac{2v_{\perp}}{\alpha_i^2} \frac{n\omega_{ci}}{k_{\perp} v_{\perp}} \right) + \frac{2v_{\parallel}}{\alpha_i^2} \left(1 - \frac{n\omega_{ci}}{\omega} \right) \right] k_{\parallel} \psi \right\} f_{0i} \quad (\text{A2})$$

and for beam ions:

$$\begin{aligned}
f_{1B} = & -\frac{e}{m_B} \sum_{n=-\infty}^{+\infty} \sum_{m=-\infty}^{+\infty} \frac{e^{i(n-m)\theta}}{(k_{\parallel} v_z - \omega + n\omega_{cB})} \\
& \times J_n(\xi_B) J_m(\xi_B) f_{0B} \\
& \times \left\{ \left[\left(1 - \frac{k_{\parallel} v_{\parallel}}{\omega} \right) \left(\frac{2v_{\perp}}{\alpha_B^2} \frac{n\omega_{cB}}{k_{\perp} v_{\perp}} - \frac{2(v_{\parallel} - V_B(X))}{\alpha_B^2} \frac{V'_B(X)}{\omega_{cB}} \right) \right] \right. \\
& + \frac{2(v_{\parallel} - V_B(X))}{\alpha_B^2} \frac{n\omega_{cB}}{\omega} \frac{k_{\parallel}}{k_{\perp}} \left. \right] k_{\perp} \phi \\
& + \left[\frac{k_{\parallel} v_{\parallel}}{\omega} \left(\frac{2v_{\perp}}{\alpha_B^2} \frac{n\omega_{cB}}{k_{\perp} v_{\perp}} - \frac{2(v_{\parallel} - V_B(X))}{\alpha_B^2} \frac{V'_B(X)}{\omega_{cB}} \right) \right. \\
& \left. + \frac{2(v_{\parallel} - V_B(X))}{\alpha_B^2} \left(1 - \frac{n\omega_{cB}}{\omega} \right) \right] k_{\parallel} \psi \left. \right\}. \quad (\text{A3})
\end{aligned}$$

Further, the perturbed number density (n) and z -component of current density (J_z) for electrons, background ions, and beam ions are derived by the substitution of perturbed distribution functions of the form Equations (A1)–(A3) into Equation (9) and are expressed as

for kappa electrons:

$$\begin{aligned}
n_e = & \frac{N_e e}{m_e} \left\{ \left[-\left(\frac{\kappa - 1}{\kappa} \right)^{1/2} \frac{1}{\omega_{ce}^2} \right] \phi \right. \\
& \left. + \left[\frac{1}{k_{\parallel}^2 \Theta_e^2} \left\{ \frac{(2\kappa - 1)}{\kappa} + \frac{i\sqrt{\pi}\kappa!}{\kappa^{3/2}\Gamma(\kappa - 1/2)} \left(\frac{2\omega}{k_{\parallel}\Theta_e} \right) \right\} \right] \psi \right\} \quad (\text{A4})
\end{aligned}$$

$$J_{ze} = \frac{N_e e^2}{m_e} \frac{\omega}{k_{\parallel} \Theta_e^2} \left\{ \frac{(2\kappa - 1)}{\kappa} + \frac{i\sqrt{\pi}\kappa!}{\kappa^{3/2}\Gamma(\kappa - 1/2)} \frac{2\omega}{k_{\parallel}\Theta_e} \right\} \psi \quad (\text{A5})$$

for background ions:

$$n_i = \frac{N_i e}{m_i} \frac{2}{\alpha_i^2} \left\{ [(1 - b_i)] \phi + \left[b_i Z' \left(\frac{\omega}{k_{\parallel} \alpha_i} \right) \right] \psi \right\} \quad (\text{A6})$$

$$J_{zi} = \frac{N_i e^2}{m_i} \left\{ \frac{\omega}{k_{\parallel} \alpha_i^2} b_i Z' \left(\frac{\omega}{k_{\parallel} \alpha_i} \right) \right\} \psi \quad (\text{A7})$$




for beam ions:

$$\begin{aligned}
n_B = & \frac{N_B e}{m_B} \left\{ \left[\frac{2}{\alpha_B^2} \frac{\bar{\omega}}{\omega} (1 - b_B) \right] \phi \right. \\
& \left. + \left[\frac{b_B}{\alpha_B^2} Z' \left(\frac{\bar{\omega}}{k_{\parallel} \alpha_B} \right) \left(1 - S \frac{k_{\perp}}{k_{\parallel}} \right) \right] \psi \right\} \quad (\text{A8})
\end{aligned}$$

$$\begin{aligned}
J_{zB} = & \frac{N_B e^2}{m_B} \left\{ \left[b_B S \frac{k_{\perp}}{\omega} \right] \phi \right. \\
& \left. + \left[\frac{\omega}{k_{\parallel} \alpha_B^2} b_B Z' \left(\frac{\bar{\omega}}{k_{\parallel} \alpha_B} \right) \left(1 - S \frac{k_{\perp}}{k_{\parallel}} \right) + S \frac{k_{\perp}}{\omega} \right] \psi \right\}. \quad (\text{A9})
\end{aligned}$$

These equations are further used in Poisson's equation and the z -component of Ampere's law to derive the dispersion relation of KAWs.

ORCID iDs

K. C. Barik  <https://orcid.org/0000-0003-3958-4587>
S. V. Singh  <https://orcid.org/0000-0003-2758-7713>
G. S. Lakhina  <https://orcid.org/0000-0002-8956-486X>

References

- Alfvén, H. 1942, *Natur*, **150**, 405
Bale, S. D., Kellogg, P. J., Mozer, F. S., Horbury, T. S., & Reme, H. 2005, *PhRvL*, **94**, 215002
Barik, K. C. 2021, PhD thesis, Indian Institute of Geomagnetism (IIG)
Barik, K. C., Singh, S. V., & Lakhina, G. S. 2019a, *PhPL*, **26**, 112108
Barik, K. C., Singh, S. V., & Lakhina, G. S. 2019b, *PhPL*, **26**, 022901
Barik, K. C., Singh, S. V., & Lakhina, G. S. 2019c, *URSB*, **2019**, 17
Barik, K. C., Singh, S. V., & Lakhina, G. S. 2020, *ApJ*, **897**, 172
Barik, K. C., Singh, S. V., & Lakhina, G. S. 2021, *ApJ*, **919**, 71
Boehm, M. H., Carlson, C. W., McFadden, J. P., Clemmons, J. H., & Mozer, F. S. 1990, *JGR*, **95**, 12157
Chandran, B. D. G., Li, B., Rogers, B. N., Quataert, E., & Germaschewski, K. 2010, *ApJ*, **720**, 503
Chaston, C. C., Peticolas, L. M., Carlson, C. W., et al. 2005, *JGRA*, **110**, A02211
Chaston, C. C., Bonnell, J. W., Clausen, L., & Angelopoulos, V. 2012, *JGRA*, **117**, A09202
Chaston, C. C., Bonnell, J. W., Halford, A. J., et al. 2018, *GeoRL*, **45**, 9344
Chaston, C. C., Bonnell, J. W., & Salem, C. 2014, *GeoRL*, **41**, 8185
Chaston, C. C., Wilber, M., Mozer, F. S., et al. 2007, *PhRvL*, **99**, 175004
Christon, S. 1987, *Icar*, **71**, 448
D'Angelo, N., Bahnsen, A., & Rosenbauer, H. 1974, *JGR*, **79**, 3129
DeCoster, R., & Frank, L. 1979, *JGR*, **84**, 5099
Delamere, P. A., Ng, C. S., Damiano, P. A., et al. 2021, *JGRA*, **126**, e28479
Duan, S., Liu, Z., & Angelopoulos, V. 2012, *ChSbu*, **57**, 1429
Eyelade, A. V., Stepanova, M., Espinoza, C. M., & Moya, P. S. 2021, *ApJS*, **253**, 34
Fried, B. D., & Conte, S. D. 2015, *The Plasma Dispersion Function* (New York: Academic)
Ganguli, G., Crabtree, C., Fletcher, A. C., et al. 2018, *NatSR*, **8**, 17186
Gary, S. P. 1986, *JPIPh*, **35**, 431
Gershman, D. J., F-Viñas, A., Dorelli, J. C., et al. 2017, *NatCo*, **8**, 14719
Goertz, C. K., & Boswell, R. W. 1979, *JGR*, **84**, 7239
Goldstein, B. E., Neugebauer, M., Zhou, X.-Y., et al. 2010, in *AIP Conf. Proc.* 1216, *Ulysses Observations of the Properties of Multiple Ion Beams in the Solar Wind* (Melville, NY: AIP), 261
Graham, D. B., Khotyaintsev, Y. V., André, M., et al. 2021, *JGRA*, **126**, e29260
Grigorenko, E. E., Sauvaud, J.-A., & Zelenyi, L. M. 2007, *JGRA*, **112**, A05218
Grison, B., Sahraoui, F., Lavraud, B., et al. 2005, *AnGeo*, **23**, 3699
Hasegawa, A. 1976, *JGR*, **81**, 5083
Hasegawa, A. 1977, *PINSA*, **86**, 151
Hasegawa, A., & Chen, L. 1976, *PhFI*, **19**, 1924
Horita, R. E., Ungstrup, E., Shelley, E. G., Anderson, R. R., & Fitzenreiter, R. J. 1987, *JGR*, **92**, 13523
Hui, C. H., & Seyler, C. E. 1992, *JGR*, **97**, 3953
Johnson, J. R., Cheng, C. Z., & Song, P. 2001, *GeoRL*, **28**, 227
Keiling, A., Wygant, J. R., Cattell, C., et al. 2002, *JGRA*, **107**, 1132
Keiling, A., Parks, G. K., Wygant, J. R., et al. 2005, *JGR*, **110**, A10S11
Keiling, A., Wygant, J. R., Cattell, C., et al. 2000, *GeoRL*, **27**, 3169
Keiling, A., Wygant, J. R., Cattell, C., et al. 2001, *JGR*, **106**, 5779
Kletzing, C. A., Scudder, J. D., Dors, E. E., & Curto, C. 2003, *JGR*, **108**, 1360
Kumar, S., Sharma, R. P., & Moon, Y.-J. 2015, *ApJ*, **812**, 69
Lakhina, G. 2008, *AdSpR*, **41**, 1688
Lakhina, G. S. 1990, *Ap&SS*, **165**, 153
Lazar, F. 2021, *Kappa Distributions* (Berlin: Springer)
Lazar, M., Fichtner, H., & Yoon, P. H. 2016, *A&A*, **589**, A39
Lazar, M., Poedts, S., & Fichtner, H. 2015, *A&A*, **582**, A124
Livadiotis, G. 2015a, *JGRA*, **120**, 880
Livadiotis, G. 2015b, *JGRA*, **120**, 1607
Livadiotis, G. 2017, *Kappa distributions: Theory and applications in plasmas* (Amsterdam: Elsevier)
Livadiotis, G., & McComas, D. 2009, *JGRA*, **114**, A11105
Louarn, P., Wahlund, J. E., Chust, T., et al. 1994, *GeoRL*, **21**, 1847
Lysak, R. L., & Carlson, C. W. 1981, *GeoRL*, **8**, 269
Maksimovic, M., Pierrard, V., & Riley, P. 1997, *GeoRL*, **24**, 1151

- Maksimovic, M., Walsh, A. P., Pierrard, V., Štverák, Š., & Zouganelis, I. 2021, Kappa Distributions; From Observational Evidences via Controversial Predictions to a Consistent Theory of Nonequilibrium Plasmas (Berlin: Springer), 39
- Makwana, K. D., Zhdankin, V., Li, H., Daughton, W., & Cattaneo, F. 2015, *PhPl*, 22, 042902
- Malaspina, D. M., Claudepierre, S. G., Takahashi, K., et al. 2015, *GeoRL*, 42, 9203
- McComas, D. J., Elliott, H. A., Schwadron, N. A., et al. 2003, *GeoRL*, 30, 1517
- McFadden, J. P., Carlson, C. W., Ergun, R. E., et al. 1998, *GeoRL*, 25, 2021
- Meziane, K., Wilber, M., Hamza, A. M., et al. 2007, *JGRA*, 112, A01101
- Moya, P. S., Gallo-Méndez, I., & Zenteno-Quinteros, B. 2021, *JASTP*, 219, 105630
- Moya, P. S., Pinto, V. A., Viñas, A. F., et al. 2015, *JGRA*, 120, 5504
- Moya, P. S., Zenteno-Quinteros, B., Gallo-Méndez, I., & Pinto, V. A. 2022, *ApJ*, 933, 32
- Narita, Y., Roberts, O. W., Vörös, Z., & Hoshino, M. 2020, *FrP*, 8, 166
- Oka, M., Ishikawa, S., Saint-Hilaire, P., Krucker, S., & Lin, R. P. 2013, *ApJ*, 764, 6
- Olbert, S. 1968, *Physics of the Magnetosphere* (Berlin: Springer), 641
- Parks, G., Chen, L. J., McCarthy, M., et al. 1998, *GeoRL*, 25, 3285
- Perri, S., Perrone, D., Yordanova, E., et al. 2020, *JPIPh*, 86, 905860108
- Phan, T. D., Bale, S. D., Eastwood, J. P., et al. 2020, *ApJS*, 246, 34
- Pierrard, V., & Lazar, M. 2010, *SoPh*, 267, 153
- Pierrard, V., & Lemaire, J. 2001, *JASTP*, 63, 1261
- Podesta, J. J., & TenBarge, J. M. 2012, *JGRA*, 117, A10106
- Procházka, O., Reid, A., Milligan, R. O., et al. 2018, *ApJ*, 862, 76
- Salem, C. S., Howes, G. G., Sundkvist, D., et al. 2012, *ApJL*, 745, L9
- Schekochihin, A. A., Cowley, S. C., Dorland, W., et al. 2009, *ApJS*, 182, 310
- Schippers, P., Blanc, M., André, N., et al. 2008, *JGRA*, 113, A07208
- Schrifer, D., Ashour-Abdalla, M., Collin, H., & Lallande, N. 1990, *JGR*, 95, 1015
- Schwadron, N. A. 2002, *GeoRL*, 29, 1663
- Shi, R., Ni, B., Summers, D., et al. 2018, *GeoRL*, 45, 5299
- Simnett, G. M. 1995, *SSRv*, 73, 387
- Štverák, Š., Maksimovic, M., Trávníček, P. M., et al. 2009, *JGRA*, 114, A05104
- Takada, T., Seki, K., Hirahara, M., et al. 2005, *JGR*, 110, A02204
- Thompson, B. J., & Lysak, R. L. 1996, *JGRA*, 101, 5359
- Ukhorskiy, A. Y., Sorathia, K. A., Merkin, V. G., et al. 2022, *NatSR*, 12, 4446
- Vasyliunas, V. M. 1968, *JGR*, 73, 7519
- Wahlund, J.-E., Louarn, P., Chust, T., et al. 1994, *GeoRL*, 21, 1831
- Wygant, J. R., Keiling, A., Cattell, C. A., et al. 2002, *JGRA*, 107, 1201
- Zastrow, M. 2016, *Eos*, 97
- Zelenyi, L. M., Dolgonosov, M. S., Peroomian, V., & Ashour-Abdalla, M. 2006a, *GeoRL*, 33, L18103
- Zelenyi, L. M., Grigorenko, E. E., Sauvaud, J.-A., & Maggiolo, R. 2006b, *GeoRL*, 33, L06105
- Zelenyi, L. M., Dolgonosov, M. S., Grigorenko, E. E., & Sauvaud, J. A. 2007, *JETPL*, 85, 187
- Zhang, L. Q., Wang, C., Dai, L., Ren, Y., & Lui, A. T. 2022, *JGRA*, 127, e2021JA029593
- Zouganelis, I. 2008, *JGRA*, 113, A08111